Contrasting stable water isotope signals from convective and large-scale precipitation phases of a heavy precipitation event in Southern Italy during HyMeX IOP13

By K. O. Lee et al.

Reply to the referees' comments

In the following, the comments made by the referees appear in black, while our replies are in red, and the proposed modified text in the typescript is in blue.

Referee #1 comments

General Comments

The authors present model simulations of isotope ratios, but there is no link to observations. Are the authors suggesting that observations from e.g. the HyMeX IOP 13 could be compared to their model results to gain additional insights? If yes, how? If not, why not just stick to a trajectory analysis? In other words, what additional insights (if any) are gained by using COSMOiso here?

In this study, a trajectory analysis based on a COSMOiso simulation has been done to investigate the moist processes in air masses associated with a heavy precipitation event (HPE) along their pathway. Stable water isotopes (SWI) experience fractionation during phase transition of hydrometeors, and hence can record information about evaporation and condensation processes during the transport of air parcels. Since the strength of fractionation depends on the meteorological conditions (temperature and saturation level), the SWI characteristics thus have led to an improved understanding of key processes affecting atmospheric humidity. Our study serves as a model-based proof of concept that such additional insights can also be obtained regarding convective precipitation events in the Mediterranean. In this way, we provide a basic motivation for future observational studies using SWI. To date, not many campaign datasets exist that would allow such observational studies yet, but with the recent advent of field deployable high precision laser spectrometric instruments, tailored field experiments become possible and will be done in the near future.

The analysis using three dimensional (3D) SWI (both $H_2{}^{16}O$ and $H_2{}^{18}O$) fields obtained from COSMOiso shown in Figures 5, 7, 8, 9, 10, 11, 12, and 13, give insights into the different moist processes occurring in the air parcels approaching Southern Italy. Especially the 3D q–δ analysis (shown in Figures 8, 9, and 12) reveal the importance of mixing, condensation, and enriching processes occurring along the moisture transport pathway. Previous studies demonstrated the usefulness of SWI to better understand meteorological processes and moisture transport, nevertheless there are still very few studies focusing on the application of SWI to investigate moist processes associated with HPEs. In particular, we see a great potential in the use of SWI for better understanding the moisture dynamics in HPEs occurring in the Mediterranean where deep convective systems are frequently observed and the origins of the moisture feeding the convection are diverse. The additional insights we can get from the COSMOiso simulation are now being more clearly emphasized in the conclusion section.

To address this, the following changes have been made.

♣ Page 16, line 1-14

"[…] We also highlight the role of the upper-level trough over the south Tyrrhenian Sea in driving the advection of the SWI-enriched plume from North Africa into the region of the deep convective system resulting in heavy precipitation over SI. Moreover, we demonstrate the importance of various moist processes such as mixing, condensation, and re-evaporation along the pathway based on the q–δ analysis using 3D SWI fields. Although our study is entirely based on a model simulation, the results suggest that the information on mesoscale moist dynamical processes and moisture transport that is contained in SWI, when combined with SWI observations, can provide very useful constraints on the representation of such processes in numerical models.

Our study is the first study to investigate the potential benefit of SWI in the context of a HPE in the Mediterranean. As such, our study provides a proof of concept of the usefulness of SWI data to understand the variety of origins and moist processes associated with air masses feeding the convection over SI. This will be further investigated in future research using SWI measurements obtained from various platforms, e.g. ground-based, near surface, airborne (Sodemann et al., 2017), and space-borne. Our modelling study will also allow designing forthcoming tailored field campaigns in the Mediterranean region."

It seems that the authors turn on a convection parameterization at 7 km horizontal resolution. Are the two parameterizations of microphysical processes consistent between the deep convection parameterization and the "large scale" microphysics parameterization? If not, how may this affect the results regarding the isotope ratios? Are the authors sure that the model skillfully represents the partitioning between parameterized and resolved precipitation or does this partitioning depend on details of the model formulation? What might be the effects of not representing this partitioning skillfully on the simulated isotope ratios? If the results were sensitive, would it even be worthwhile to try to improve the partitioning in the model or should one just wait until deep convection parameterizations become obsolete?

Of course the partitioning between convective and large-scale precipitation is somewhat artificial (there is not such separation in observations) and depends on the model as well as on the resolution (when going to finer resolutions, the model explicitly resolves a larger portion of the mesoscale convective activity). However, this partitioning is not the main aspect/goal of our study. In addition, we are confident that the current model setup is well-suited for the purpose of exploring the worth of isotope data for understanding mesoscale moist processes.

The grid spacing of 7 km together with the Tiedtke convection scheme were used for operational predictions at the German Weather Service DWD for a long time, such that the model is very well tuned in this configuration. We also chose this relatively coarse resolution because it allows for a large model domain that reduces the dependence on the much coarser isotope boundary data (spectral resolution of T62 in IsoGSM) and enables us to calculate backward trajectories consistently over longer periods.

I must admit that I do not fully understand the purpose of this manuscript. To me this study raises more questions than it answers. Major revisions will be necessary before I can recommend this study for publication.

We appreciate the time and effort you put in this review as well your mindful comments on our paper. In this study, using the hourly 3-D water vapour isotope data, we highlight the large variety of moisture sources and transport pathways that induced the two precipitation phases, and the isotopic characteristics of various air masses associated with upper-level trough, cold front, mistral, and African moist plume, that were involved in convection development. Although our study is entirely based on a model simulation, the results suggest that the information on mesoscale moist dynamical processes and moisture transport that is contained in SWI, when combined with SWI observations, can provide very useful constraints on the representation of such processes in numerical models. As such, our study provides a proof of concept of the usefulness of SWI data to understand moist processes associated with a Mediterranean heavy precipitation event with diverse origins and pathways of moisture feeding the convection. We have worked hard to comply with all of them. Replies to each comment are listed below.

Specific comment

1. Title and abstract: based on the title and abstract I would have somehow expected a connection with observations. The title should explicitly state that this is purely a modelling exercise.

Agreed. We have modified the title and abstract accordingly.

♣ Page 1, line 2-3 (title)

"Contrasting stable water isotope signals from convective and large-scale precipitation phases of a heavy precipitation event in Southern Italy during HyMeX IOP 13: a modelling perspective"

♣ Page 1, line 15-17 (abstract)

"The dynamical context and moisture transport pathways embedded in large scale flow and associated with a heavy precipitation event (HPE) in Southern Italy (SI) are investigated with the help of stable water isotopes (SWIs) based on a purely numerical framework."

2. Given that this is purely a modelling exercise, I would have expected either some sensitivity studies or else a more explicit description on how the model results presented here might be linked to either existing or to future observations.

Agreed. Although our study is entirely based on a model simulation, the results suggest that the information on mesoscale moist dynamical processes and moisture transport that is contained in SWI, when combined with SWI observations from various platforms (also our response to the first general comment), can provide useful constrains on the representation of such processes in numerical models. In fact, several field campaigns involving SWI measurements are planned in the Mediterranean region.

♣ Page 16, line 9-14

"Our study is the first study to investigate the potential benefit of SWI in the context of a HPE in the Mediterranean. As such, our study provides a proof of concept of the usefulness of SWI data to understand the variety of origins and moist processes associated with air masses feeding the convection over SI. This will be further investigated in future research using SWI measurements obtained from various platforms, e.g. ground-based, near surface, airborne (Sodemann et al., 2017), and space-borne. Our modelling study will also allow designing forthcoming tailored field campaigns in the Mediterranean region."

3. Is the main point of this study a simulation of a quantity that has not been observed or are there fundamental new results that cannot be found in the existing literature? If this is the case, these points should at least briefly be discussed in the light of the existing literature.

Current SWI measurements are mainly obtained from space-borne retrievals (e.g. Schneider et al. 2017, Lacour et al., 2017) and ground-based in-situ laser spectroscopy (e.g. Aemisegger et al. 2012) as well as from monthly precipitation samples at various stations (GNIP; IAEA, 2006). The space-borne measurements provide continuous datasets in space at the global scale with coarse vertical resolution and limited precision. On the other hand, ground-based measurements with high temporal resolution are only available from a few locations and from dedicated field campaigns. In particular, the data availability for the Mediterranean region is very limited. A notable exception is the airborne dataset acquired around Corsica during the HyMeX SOP1 (Sodemann et al., 2017). However, it does not include SWI observations for the days under scrutiny in this paper. Due to these limitations, we use a model to demonstrate the usefulness of SWI data for understanding moist processes associated with a Mediterranean HPE. In this way, we provide a motivation and justification for future measurement efforts dedicated to this topic. As mentioned above, we have extended the conclusion section to make this clearer.

♣ Page 4, from line 23 (introduction)

"SWI measurements are mainly obtained from space-borne retrievals (e.g. Schneider et al., 2016; Lacour et al., 2017) and ground-based in-situ laser spectroscopy (e.g. Aemisegger et al., 2012). The space-borne measurements provide continuous datasets in space at the global scale with coarse vertical resolution and limited precision. On the other hand, ground-based measurements with high temporal resolution are only available from a few locations and from dedicated field campaigns. In particular, the data availability for the Mediterranean region is very limited. A notable exception is the airborne dataset acquired around Corsica (Sodemann et al., 2017) during the first Special Observing Period of the Hydrological cycle in the Mediterranean Experiment (HyMeX SOP-1, Ducrocq et al., 2014). However, it does not include SWI observations for the days under scrutiny in this paper. Due to these limitations we use a model to demonstrate the usefulness of SWI data for understanding moist processes associated with a Mediterranean HPE."

♣ Page 16, line 5-14 (conclusion)

"[…]Although our study is entirely based on a model simulation, the results suggest that the information on mesoscale moist dynamical processes and moisture transport that is contained in SWI, when combined with SWI observations, can provide very useful constrains on the representation of such processes in numerical models.

Our study is the first study to investigate the potential benefit of SWI in the context of a HPE in the Mediterranean. As such, our study provides a proof of concept of the usefulness of SWI data to understand the variety of origins and moist processes associated with air masses feeding the convection over SI. This will be further investigated in future research using SWI measurements obtained from various platforms, e.g. ground-based, near surface, airborne (Sodemann et al., 2017), and space-borne. Our modelling study will also allow designing forthcoming tailored field campaigns in the Mediterranean region."

4. Why was COSMOiso used and not just a simple trajectory analysis?

The additional insights we can get from COSMOiso simulation has been emphasized in conclusion section, as explained in the answer to the first general comment. The added value of an isotope enabled numerical simulation of this HPE event compared to a purely trajectory based study on moist processes, is that mixing, convective and cloud processes are included in a more detailed way. Trajectory-based studies have been done to investigate the contribution of different evaporative moisture sources for precipitation events (e.g. Sodemann and Zubler, 2010). But it is not straightforward to assess the relevance of different dynamical processes involved in moisture transport pathways solely based on trajectories. This is why a more sophisticated modelling approach is employed here.

Contrasting stable water isotope signals from convective and large-scale precipitation phases of a heavy precipitation event in Southern Italy during HyMeX IOP13

By K. O. Lee et al.

Reply to the referees' comments

In the following, the comments made by the referees appear in black, while our replies are in red, and the proposed modified text in the typescript is in blue.

Referee #2 comments

General Comments

A case study of a heavy precipitation event over southern Italy during HyMeX IOP13 in October 2012 has been discussed by far-reaching and detailed interpretation of model output. However the only validation of the results presented are numerous rain-gauge data from stations in southern Italy. Although the analysis of the model results are sophisticated and as far as possible reliable and in accordance with known synoptic and sub-synoptic flow pattern, any link to real processes is missing due to missing observations.

By the title the authors guide the reader to a case study of combined convective and large scale precipitation formation. But this is only partly the case. Studying the manuscript we can learn, that with the use of the selected models, how much in detail we can interpret and consequently use the COSMOiso model for small scale precipitation analysis and thus for forecasting issues. This should clearly be indicated in the title and it should be stated in the abstract that trajectory calculation and simulated stable water isotope analysis give valuable additional information for weather interpretation and forecasting purposes. The authors are asked to rephrase the title accordingly and to rewrite the abstract and conclusions. Otherwise, a case study based on model data only and without any supporting data (with the exception of the precipitation data) is not sufficient for publication.

Agreed. This study is entirely based on model simulations. We have been looking at SWI measurement obtained from space-borne retrievals, the Infrared Atmospheric Sounding Interferometer (IASI). IASI measurements provide continuous datasets in space at the global scale with coarse vertical resolution and limited precision. A recent retrieval algorithm (Lacour et al., 2017) provides δD in the middle troposphere (3-6 km column) with an error of 38 ‰ in cloud free regions. Figure A shows the IASI-retrieved δD and q maps of the western Mediterranean on 15 October 2012. The enriched air mass (δD ≥ –150 ‰, q ≥ 7 g kg^{-1}) is captured by IASI in the strait of Sicily (around 12–22°E, 30–38°N), as similarly as seen in COSMOiso simulation (see Figure 4 of manuscript).

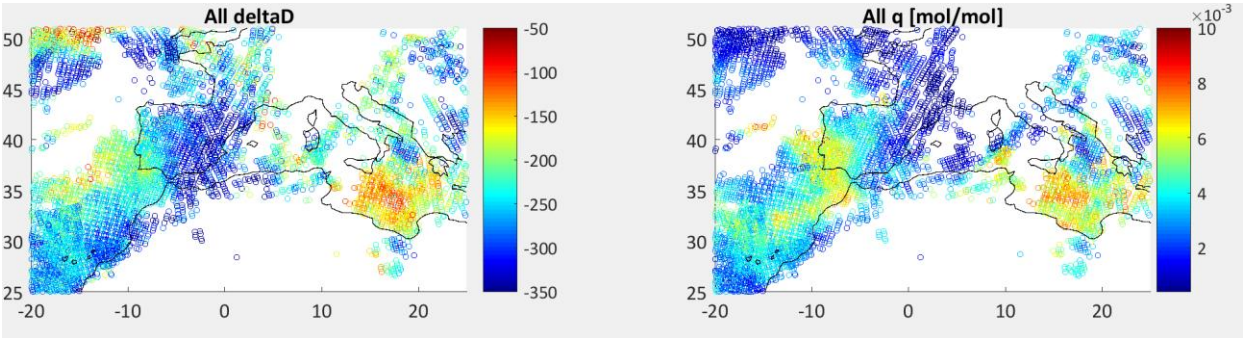

Figure A. Maps of δD (left) and q (right) measured by IASI on 15 October 2012 (both morning and evening orbit).

When comparing the IASI-retrieved δD and COSMOiso-derived δD in the western Mediterranean region (-10–25°E, 25–45°N) we see the IASI retrievals are biased high by more than 30 ‰ (Figure B). This comparison shows a reasonable agreement between IASI and COSMOiso, in spite of the bias. However, due to the temporally and spatially limited sample of IASI products associated with a single convection event, we have decided to use purely a modelling approach to demonstrate the usefulness of SWI data for understanding moist processes associated with a HPE. Correspondingly, the title, abstract, introduction, and conclusion have been corrected to specify this. Nevertheless, the comparison between IASI and COSMOiso provides a motivation for future studies to demonstrate the long-term (monthly to seasonal) SWI characteristics in connection to the HPE in the western Mediterranean basin.

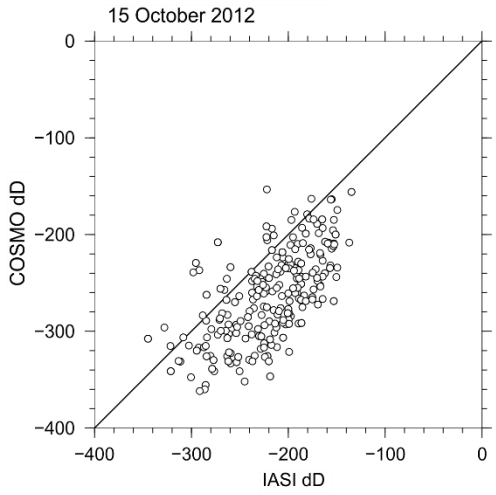

Figure B. The IASI-retrieved δD and COSMOiso-produced δD in the western Mediterranean region on 15 October 2012 (both morning and evening orbit).

Accordingly, the following changes have been made:

♣ Page 1, line 2-3 (title)

"Contrasting stable water isotope signals from convective and large-scale precipitation phases of a heavy precipitation event in Southern Italy during HyMeX IOP 13: a modelling perspective"

♣ Page 1, line 15-17 (abstract)

"The dynamical context and moisture transport pathways embedded in large scale flow and associated with a heavy precipitation event (HPE) in Southern Italy (SI) are investigated with the help of stable water isotopes (SWIs) based on a purely numerical framework."

♣ Page 4, from line 23 (introduction)

"SWI measurements are mainly obtained from space-borne retrievals (e.g. Schneider et al., 2016; Lacour et al., 2017) and ground-based in-situ laser spectroscopy (e.g. Aemisegger et al., 2012). The space-borne measurements provide continuous datasets in space at the global scale with coarse vertical resolution and limited precision. On the other hand, ground-based measurements with high temporal resolution are only available from a few locations and from dedicated field campaigns. In particular, the data availability for the Mediterranean region is very limited. A notable exception is the airborne dataset acquired around Corsica (Sodemann et al., 2017) during the first Special Observing Period of the Hydrological cycle in the Mediterranean Experiment (HyMeX SOP-1, Ducrocq et al., 2014). However, it does not include SWI observations for the days under scrutiny in this paper. Due

to these limitations, we use a model to demonstrate the usefulness of SWI data for understanding moist processes associated with a Mediterranean HPE, for the first time."

♣ Page 16, from line 5 (conclusion)
"[…] Although our study is entirely based on a model simulation, the results suggest that the information on mesoscale moist dynamical processes and moisture transport that is contained in SWI, when combined with SWI observations, can provide very useful constrains on the representation of such processes in numerical models.

Our study is the first study to investigate the potential benefit of SWI in the context of a HPE in the Mediterranean. As such, our study provides a proof of concept of the usefulness of SWI data to understand the variety of origins and moist processes associated with air masses feeding the convection over SI. This will be further investigated in future research using SWI measurements obtained from various platforms, e.g. ground-based, near surface, airborne (Sodemann et al., 2017), and space-borne. Our modelling study will also allow designing forthcoming tailored field campaigns in the Mediterranean region."

After redirection the scope of the paper, precipitation process information based on trajectory and SWI model output can be a helpful tool to examine actual weather situations governed by mutual evaporation-condensation processes. This is relevant scientific research and within the scope of ACP as the paper introduces additional parameters in operational weather analyses. The relevant SWI literature is cited by the authors, and the model set up is explained sufficiently. The analysis of the model results is accurate and detailed. The description of the flow field and the evaporation-condensation cycle are reliable. The structure of the paper is comprehensible. Some comments on figures, abbreviations, text etc. see "minor points".
I recommend the paper for publication in ACP after redirecting the purpose of the paper.
We appreciate the time and effort you put in this review as well your mindful comments on our paper. We have worked hard to comply with all of them. Replies to each comment are listed below.

Minor comment

1. P1, L15 (new): Moisture transport pathways embedded in large scale flow and associated…
Corrected.

2. P2, L26: The paper "Diagnostic study of a HyMeX heavy precipitation event over Spain by investigation of moisture trajectories (Rohner, L., Nerding, K.-U., Corsmeier, U., 2016, Quarterly journal of the Royal Meteorological Society)" shows the analysis of a HPE by combination of simulations and observations including moisture trajectories. In "Sodemann et al. (2017)" the potential of airborne measurements of SWI (during HyMeX) is shown.
Thanks for noting the reference of Röhner et al., 2016. We have included the paper in the reference list (P2, L27), while Sodemann et al. (2017) and the potential of airborne measurement of SWI have been emphasized in P16, L14.

3. P3, L15: better: … condensation cycles during…
Corrected.

4. P3, L20: explain the expression in brackets in a separate sentence for better readability.
Corrected.

♣ From Page 3, line 19

"[…] For instance, low δ^2H (typical range between –160 and –180 ‰) or $\delta^{18}O$ (i.e. range between –20 and –30 ‰) values in atmospheric water vapour at surface indicate low air mass temperatures and strong rainout of air parcels (e.g. Jacob and Sonntag, 1991; Yoshimura et al., 2010), whereas high δ^2H (typical range between –120 and –100 ‰) or $\delta^{18}O$ (range between –18 and –14 ‰) indicate high air mass temperatures and recent admixture of fresh ocean evaporate. The δ notation describes the concentrations of the heavy isotopes relative to the isotope ratio of the Vienna Standard Mean Ocean Water– RVSMOW, by for instance, $\delta^{18}O = (Rs/RVSMOW – 1) \times 1000$, where $Rs = [H_2{}^{18}O]/[H_2{}^{16}O]$ is the isotope ratio of a water sample."

5. P4, third paragraph: abbreviations SI, IOP, P1, and P2 have been explained before in the abstract.
The abstract and the main text should be considered as 2 separate entities. Hence, acronyms need to be defined in the main text, even if they already appear in the abstract.

6. P6, L21: refer to Fig. 1
Corrected.

7. P6, L26: refer to Fig. 2
Corrected.

8. P8, L13: … transported from northern Africa…
Corrected.

9. P8, L15: isn't it 314−330 K instead of 308−326 K?
Corrected to 315−330 K with improved color scale of Fig. 3.

10. P8, L23: isn't it western edge of the Ty-box instead of north-eastern edge?
Corrected to western edge.

11. P8, last paragraph: this paragraph should be removed to section 4
Thanks for suggestions. The paragraph has been moved to the beginning of section 4.

12. P9, L9: The cold front is often mentioned in the text but never indicated in the figures (with exception of Fig. 14, conceptual model).
Agreed. The cold front is indicated where potential temperature (ϑ) values show a large gradient (315–330 K) at 850 hPa and it is marked by a dashed line in right panels of Fig. 3.

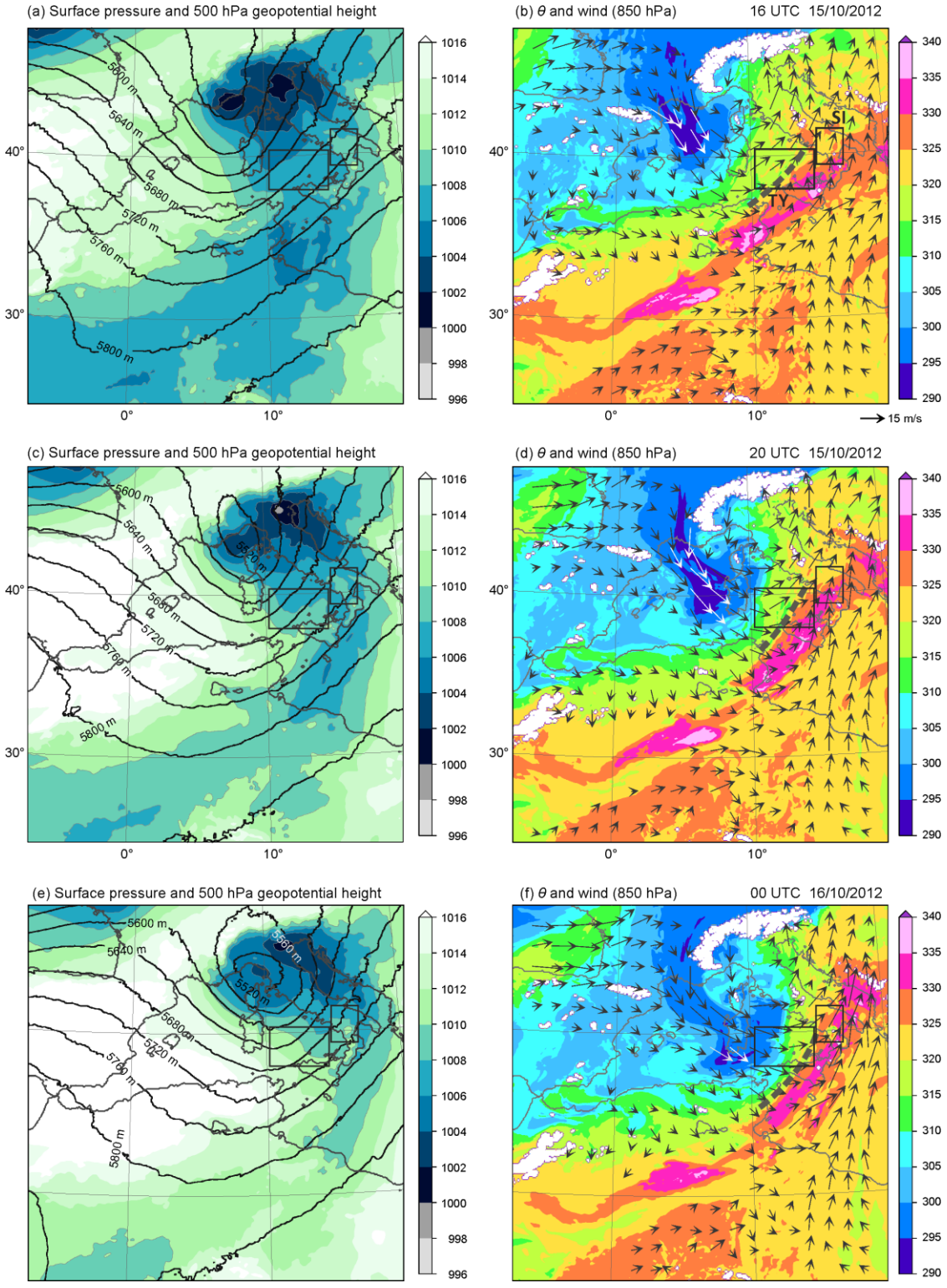

Figure 3. Horizontal distributions of sea level pressure (shading) and geopotential height at 500 hPa (contours) (left), and potential temperature, ϑ (shading), and wind (black and white arrows) at 850 hPa (right) at 16 UTC (top) and at 20 UTC (middle) 15 October 2012, and 00 UTC on 16 October 2012 (bottom) produced by the COSMOiso simulation. Coastal line is depicted by black line. The location of cold front is depicted by a dashed line in right panels.

13. Section 4.1: The caption “Distribution of SWIs… prior to HPE” does not fit to the text: the interval with precipitation (16 UTC to 07 ITC) is discussed in this paragraph.
Agreed. We have restructured Sections 3 and 4. Section 4.1 has been combined with section 3, and the corresponding new subsection is entitled “Distribution of SWIs over the Mediterranean”.

14. P12, L15: Figs. 8c and 8d do not exist.
Corrected to Figs. 10c, d.

15. P14, L24: … (grey encapsulated area in Fig. 14a). In the figure the area is called “blue encapsulated”.
Corrected consistently to “green encapsulated area”.

16. Figure 3: use isobars for showing the surface pressure field. Indicate the position of the cold front.
The sea surface isobar and geopotential height at 500 hPa have been shown in the left panels of Figure 3 to show the upper level trough. In the right panels, the horizontal wind at 850 hPa is indicated together with ϑ at 850 hPa, while the position of cold front is defined by a large ϑ gradient of 315–330 K (please see our reply for comment #12).

17. Figure 5: skip the upper and middle color bars.
As suggested the color scale has been adjust for sake of readability. With a suggestion from other referee, sections 3 and 4 have undergone restructuring to describe the core results more concisely. By this, Figure 5 have been re-ordered to Figure 4.

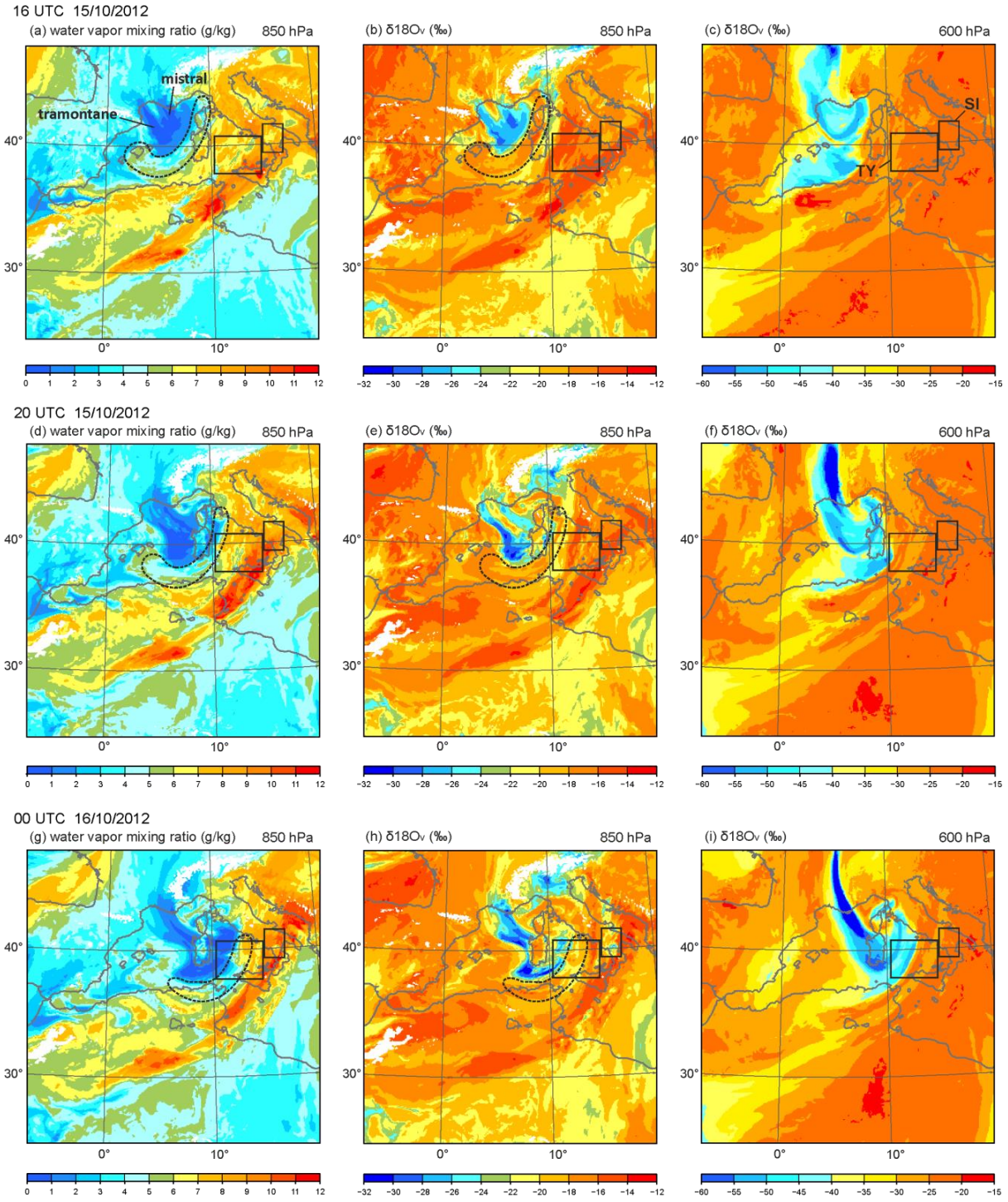

Figure 4. Horizontal distributions of water vapour mixing ratio at 850 hPa (left), $\delta^{18}O_v$ at 850 hPa (middle) and $\delta^{18}O_v$ at 600 hPa (right) at 16 UTC (top) and 20 UTC (middle) on 15 October 2012, and 00 UTC on 16 October 2012 (bottom).

18. Figure 8: a color bar is missing.

The color bar is now added to Figure 8.

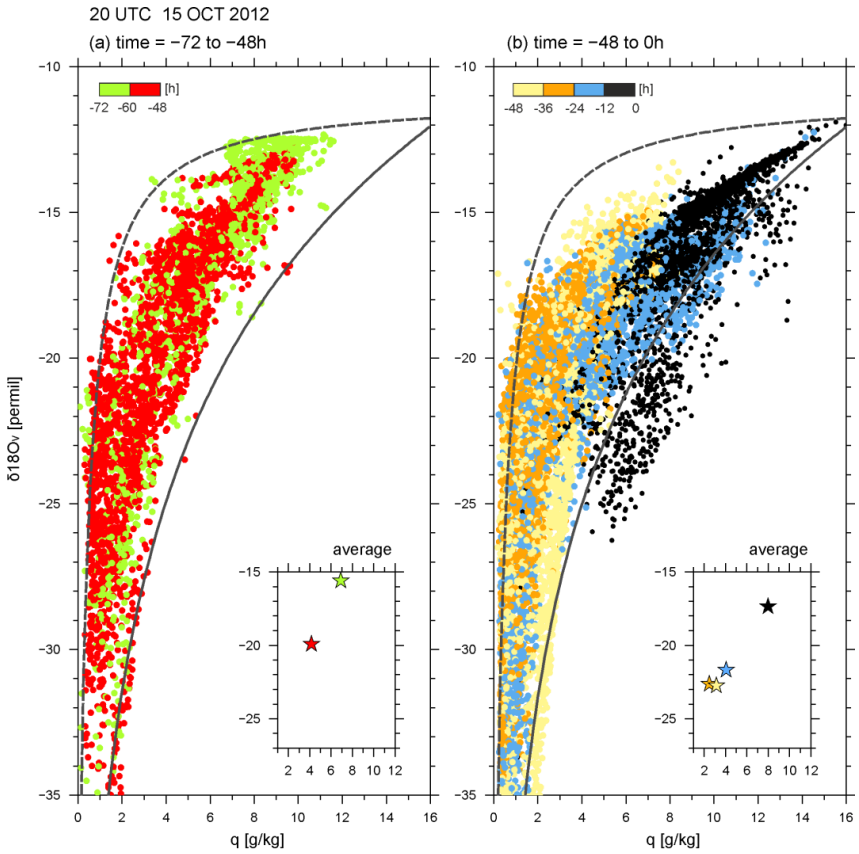

Figure 8. Scatter diagram of q and $\delta^{18}O_v$ along the backward trajectories of Figure 7 during (a) the times between −72 and −48 h, and (b) times between −48 and 0 h every 12 hours from 20 UTC on 15 October 2012. The colour of dot changes every 12 h. The mixing and Rayleigh lines are indicated in each panel by dashed and solid line, respectively. The averaged q and $\delta^{18}O_v$ every 12 hours is displayed in the bottom right corner of each panel.

19. Figure 10: changing color bars for the sub-figures makes it difficult to interpret figure differences.
As suggested, a single color bar has been used for plots related to $\delta^{18}O_v$ (Fig. 10b, d, and f), and a single color bar was used $\delta^{18}O_r$ (Fig. 10c, e) and $\delta^{18}O_s$ (Fig. 10g).

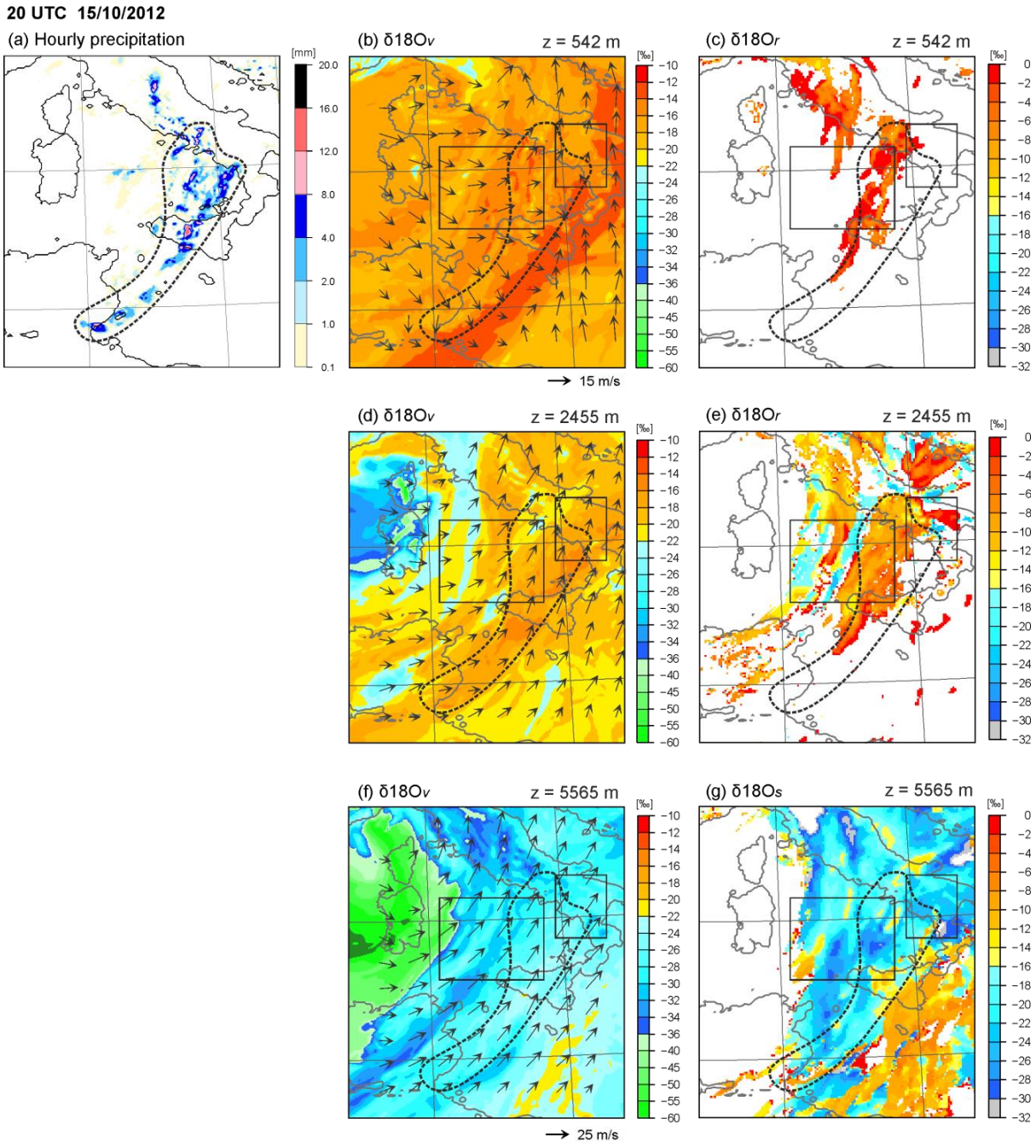

Figure 10. Horizontal distributions of (a) surface hourly precipitation (mm), $\delta^{18}O_v$ (‰) at (b) model level 8 (about 542 m ASL), (c) model level 16 (about 2455 m ASL), and (d) model level 23 (about 5565 m ASL, $\delta^{18}O_r$ (‰) at (e) 542 m ASL and (f) 2455 m ASL, and $\delta^{18}O_s$ (‰) at 5565 m ASL at 20 UTC on 15 October 2012. Note that, due to the terrain-following coordinates, the SWI values are partly depleted over topography, e. g. in central Italy. The precipitating area is marked by the area enclosed by the dashed line.

20. Figure 13: as Fig. 10

Figure 13 has been improved in the same way of Figure 10.

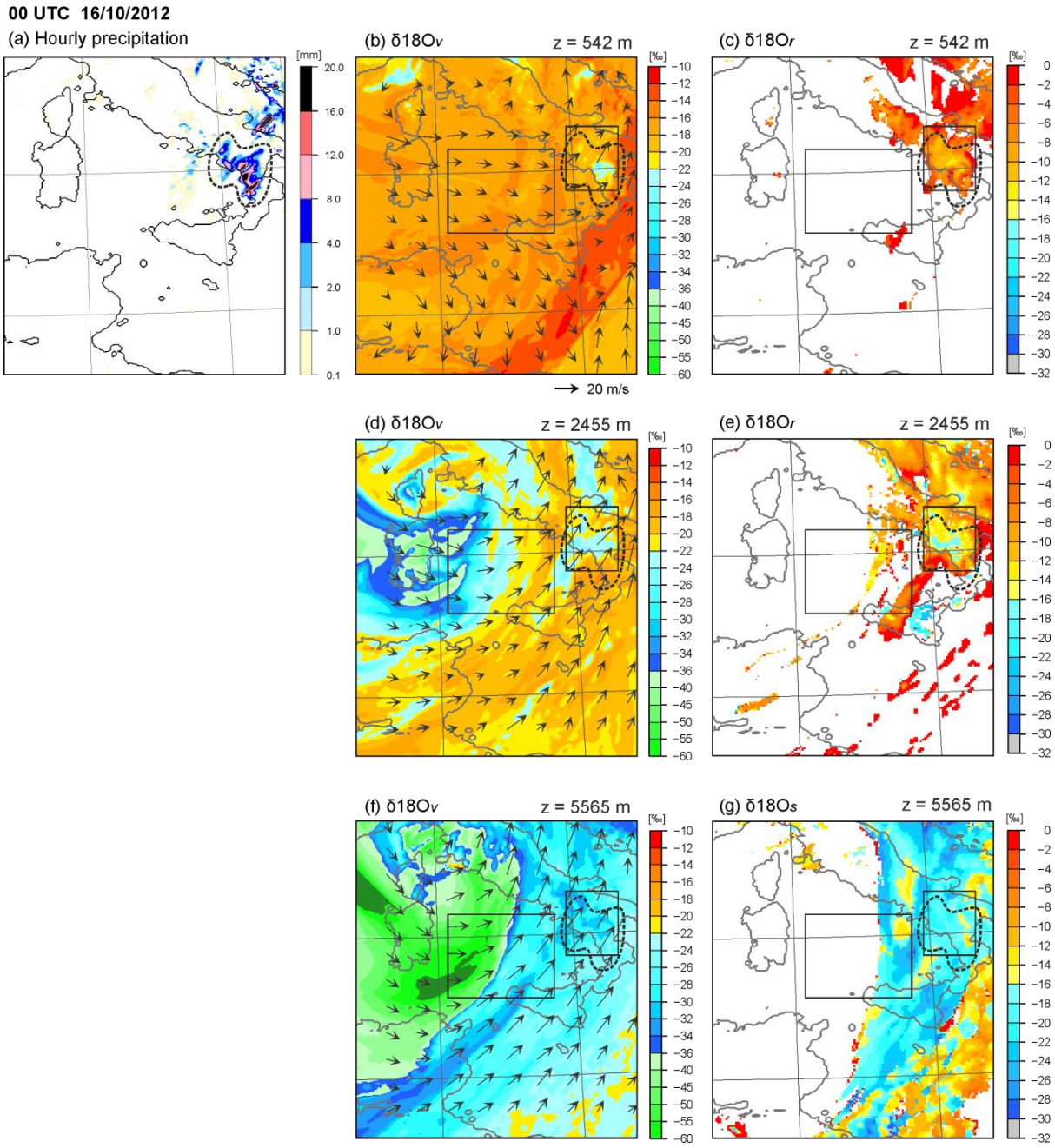

Figure 13. Same as Figure 10 but for 00 UTC on 16 October 2012.

21. Figure 14: the color differences (grey, blue, yellow shading) is difficult to read if manuscript is printed. Corrected to green, yellow, and red shading for better readability.

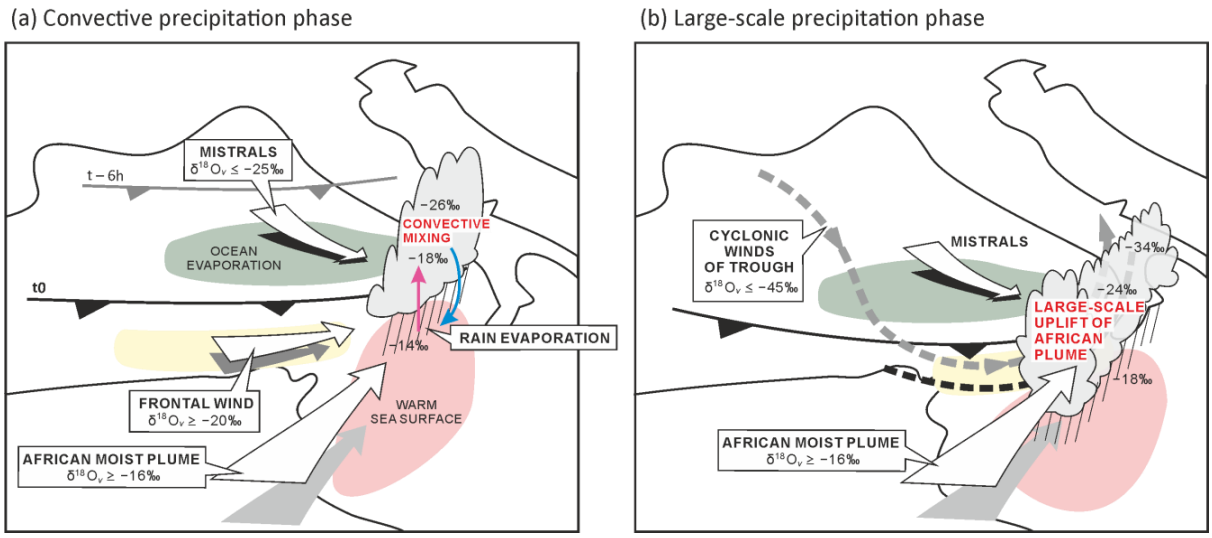

Figure 14. Schematics summarizing the main processes and the key features of water vapour isotopologues associated with deep convection upstream of SI and leading to the Phase 1 (a) and Phase 2 (b) of the HPE. In (a) and (b), white descending arrow indicate the mistral wind behind the edge of the cold front (thick black line). The white arrow in the yellow-shading encapsulated area illustrates the frontal wind at 850 hPa, and the white arrow in the red-shading encapsulated area (warm sea surface) indicates the elevated African moist plume. In (a), convective ascent and precipitating downdraft are depicted by red and blue arrows, respectively. In (b), the southern edge of upper trough is indicated by black dashed line and the cyclonic flow of the trough is indicated by grey dashed line.

Contrasting stable water isotope signals from convective and large-scale precipitation phases of a heavy precipitation event in Southern Italy during HyMeX IOP13

By K. O. Lee et al.

Reply to the referees' comments

In the following, the comments made by the referees appear in black, while our replies are in red, and the proposed modified text in the typescript is in blue.

Referee #3 comments

General Comments

The reviewed article is a thorough case study performed using COSMOiso. While the analysis of the simulation results is highly detailed, the title and abstract of the manuscript lead the reader to expect a comparison to observations. However, the only observations used are precipitation measurements. Considering the emphasis on isotope modelling, I would have expected at least some measurements of this nature. For that reason, the purpose of the manuscript as a whole, and especially the long and detailed analysis of isotope distributions within the manuscript, is not clear.

The main question is: what additional insight is gained from the use of a model-only isotope analysis. This problem is further underlined by the presented trajectory analysis, which seems to provide the same information which is derived from the isotope concentrations. For a recommendation for publication, the authors need to better outline the purpose of the study, as well as their reasoning for using COSMOiso and its advantages compared to a trajectory analysis or even just passive tracers.

Assuming these problems can be addressed, a number of other issues remain. Below is a detailed listing of major and minor comments which should help the authors to improve their manuscript substantially.

We appreciate the time and effort you put in this review as well your mindful comments on our paper. We have worked hard to comply with all of them. Replies to each comment are listed below.

Major comment

1. Section 4 is the core of the manuscript. However, even considering that, it seems out of proportion. It is not only very long but also difficult to read and descriptive over long spans. This sections would greatly benefit from being shorter and more concise.

Agreed. Sections 3 and 4 have undergone restructuring to describe the core results more concisely. The previous section 4.1 has been combined with section 3 to avoid the repetition about the synoptic context. Section 3 is now entitled "Overview of meteorological condition" with two subsections: "3.1 One HPE with two precipitation phases over southern Italy", and "3.2 Distribution of SWI over the Mediterranean". Sections 4 is now entitled "SWI distribution during two precipitation phases" with two subsections of "4.1 The convective phase of precipitation", and "4.2 The large-scale phase of precipitation".

2. Parts of the conclusion repeat contents of section 4 in too much detail, shorten and be much more concise and clear.

Agreed. The conclusion is now more concise after removing the content redundant with section 4.

♣ Page 15, from line 8 (conclusion)

"The 3-day backward trajectory analysis shows that the air parcels arriving in SI during P1 originate from the North Atlantic and descend within the upper-level trough over the north-western Mediterranean Sea. The SWI-depleted air mass (median $\delta^{18}O \leq -45$ ‰) within the descending air parcels ~~arriving at very low levels (below 1 km) are very dry and SWI depleted ($\delta^{18}O \leq -25$‰, water vapour mixing ratio, $q \leq 2$ g kg^{-1}), and~~ rapidly take up a large amount of water vapour from ocean evaporation (green encapsulated area in Fig. 14a)~~). As a consequence, it becomes enriched in SWI ($\delta^{18}O \geq -14$‰) in a very short time span~~ over the Tyrrhenian Sea and also from evaporated moisture from falling precipitation~~ as hinted by the analysis of the trajectory data in the q–δ space (points falling below the Rayleigh distillation line)~~. Additional moisture is taken up over the Strait of Sicily~~ at altitudes below 2 km ASL~~ from mixing with the enriched moisture plume coming from Africa ($\delta^{18}O_v \geq -16$ ‰). The SWI-enriched low-level air masses arriving upstream of SI are convectively pumped to higher altitudes, producing precipitation over SI, and the SWI-depleted moisture is transported towards the surface within the downdrafts ahead of the cold front (red and blue arrows, Fig. 14a).

During P2 (Fig. 14b), just a few hours after P1, the origin of the air parcels arriving at SI is distinct, i.e. mostly from North Africa. The air parcels are moist and associated with large $\delta^{18}O$ values (bottom most arrow, median $\delta^{18}O_v \geq -16$ ‰~~, median $q \geq 6$ g kg^{-1}~~). With the arrival of the upper-level trough ($\delta^{18}O_v \leq -45$ ‰~~ at 600 hPa~~) and ~~low level~~ mistral ($\delta^{18}O_v \leq -25$ ‰~~ at 850 hPa~~) over the southern Tyrrhenian Sea, the strong cyclonic flow around the trough (grey dashed line in Fig. 14b) induces the advection of the moist plume towards SI and leads to large-scale uplift of the warm and moist African air mass along the cold front. It brings moisture and leads to gradual rain out of the air parcels over Italy~~ (following Rayleigh distillation)~~. For the convective precipitation phase (P1), most of the moisture processes producing the HPE take place during the last 18 hours before the arrival over SI, while the large-scale advection of SWI-enriched moisture from the African plume by strong cyclonic flow lasts about 72 hours during the large-scale precipitation phase (P2).~~ In both phases, the air parcels take up substantial amount of water vapour over the Mediterranean."

3. The authors need to discuss their results in a critical way which includes an explanation of the insights gained by using COSMOiso over a normal mesoscale simulation, which would be possible at a much higher resolution too. This discussion can be part of the last section Conclusions and Discussion.

The chosen setup (COSMOiso simulation with 7 km grid spacing and parameterized convection) is a tradeoff between high enough resolution for including detailed dynamics of the mesoscale systems and still being able to run efficiently over a large domain that also includes the moisture plume over North Africa. Also this selected resolution and large model domain reduce the dependence on the much coarser isotope boundary data (spectral resolution of T62 in IsoGSM) and enables us to calculate backward trajectories consistently over longer periods. This discussion is added in section 5, Conclusion.

♣ Page 16, from line 14

"[…] In this study, COSMOiso simulation at a horizontal grid spacing of about 7 km with parameterized convection results from a trade-off between having high enough resolution for including detailed dynamics of the mesoscale systems and being able to run efficiently over a large domain (about 4300 km × 3500 km) that includes the moisture plume over North Africa. This setup allows addressing the question we are interested in, namely: which isotope signals are due to local processes, and which are due to large-scale advection? To further study the details of the fractionation processes in and around deep convective systems, complementary investigations will be conducted using higher resolution convection-permitting simulation with a 2 km grid to shed a light on cloud microphysical processes inside deep convection."

4. Multiple figures are difficult to read, be it due to bad coloring or their size. The authors could greatly improve the manuscript's readability by making sure that figures use more contrasting color table, fewer contour levels and that the figure size and shape make better use of the available space. I mention specifics for certain figures throughout the minor comments, but the other figures can also be improved following those same guidelines.
Agreed. We have improved Figures 1, 3, 5, 8, 10, 12, 13, and 14 for better readability.

5. Figures are often referenced out of order, try to keep this to an absolute minimum. This will likely require some restructuring of the text.
The order of reference of Figures is now corrected throughout the paper.

Minor comment

1. P3, L1: large amounts of water vapor. How large?
Corrected.

♣ Page 3, from line 1
"[…] the intrusion of large amounts of moisture, about one quarter of the total integrated water vapour, […]"

2. P3, L10: observations of the most stable water isotopes alone can be limited this indicates that "normal" observations only look at this isotopes, but I assume that the sentence refers to classical observations which simply look at the total moisture without any regard for different isotopes. This should be more clear.
Corrected to "the SWI observation of other, less abundant SWIs, i.e. $H_2{}^{18}O$ and $HD^{16}O$".

3. P3, L14-15: replace *in the other phase (vapor)* with just *in vapor*
Corrected.

4. P3, L19-24: Please specify what *high* and *low* are in this context by giving typical values
The typical ranges of each values are indicated by referring to Jacob and Sonntag (1991) and Yoshimura et al. (2010).

♣ Page 3, line 19-23
"[…] For instance, low δ^2H values (typically ranging between –160 and –180 ‰) or low $\delta^{18}O$ values (i.e. ranging between –20 and –30 ‰) at the surface indicate air masses characterized by low temperatures and strong rainout of air parcels (e.g. Jacob and Sonntag, 1991; Yoshimura et al., 2010), whereas high δ^2H values (typically ranging between –120 and –100 ‰) or high $\delta^{18}O$ values (ranging between –18 and –14 ‰) indicate air masses characterized by high temperatures and recent admixture of fresh ocean evaporate."

5. P3, L29: remove commas
Removed.

6. P4, L16: change to *used **a** stable isotopic* or *used stable isotopic signal**s***
Corrected to "used stable isotopic signals".

7. P4, L20: add comma after mesoscale
Added.

8. P4, L25-27: move the part *that occurred (…) Mediterranean Experiment (HyMeX …)* to a separate sentence
Corrected while the acronyms of HyMeX has been defined in the previous paragraph.

♣ Page 5, line 7-10
"[…] The target HPE occurred during the Intensive Observation Period 13 (IOP 13) of the HyMeX SOP-1. Using a combination of ground-based, airborne and space-borne observations and numerical simulations of this HPE, Lee et al. (2016) investigated the detailed dynamic and thermodynamic environments of the two precipitation phases of the HPE."

9. P5, L1-5: This description is difficult to follow if one is not familiar with Lee et al. (2016). This should be moved to section 3, where it can make use of Figs. 1-3 for a thorough but concise description of the event (see also comments on Fig. 1)
Agreed. The description about Lee et al. (2016) has been moved to section 3.2.

♣ Page 9, line 2-7
"The moisture structure upstream of the HPE; 1) the presence of an African moisture plume favouring the efficiency of the convection to produce more precipitation, 2) the importance of southerly flow from the warmer Mediterranean Sea south of Sicily in enhancing the convergence ahead of the cold front, and 3) the role of the upper-level trough over southern France extending to the western Mediterranean in organizing convection at the leading edge of the surface front, highlighted by Lee et al. (2016) has been further studied using SWI data […]"

10. P5, L3: remove *wind* after *mistral*
Corrected.

11. P5, L4: change *convection activity* to *convective activity*
Corrected.

12. P5, L8: add *and* after the comma
Added.

13. P5, L10: change to *However, the origin and transport pathways of moisture have not been studied to date*
Corrected.

14. P6, L2: specify that this is a *deep* convection scheme, since the resolution of the model has not yet been mentioned at this point
Specified.

15. P6, L3: please add a very brief and concise description of what these physics and isotope parametrizations do, one to three sentences should suffice.
A brief description of isotope physics and parametrizations has been included.

♣ Page 6, line 7-18
"[…] All prognostic moisture fields, which are simulated by the model in terms of specific humidities, are duplicated

twice, representing the specific humidities of $H_2{}^{18}O$ and $HD^{16}O$, respectively. From the prognostic specific humidity fields, the isotope ratios in usual δ-notation can be calculated. The heavy isotopes experience the same processes as the light isotope ($H_2{}^{16}O$), except during phase transition, when isotopic fractionation occurs. A one-moment microphysics scheme is used and deep convection is parameterised following Tiedtke (1989). In the microphysical scheme, transfer rates between the different water species during the formation of clouds and precipitation are specified. The heavy isotopes are affected by equilibrium fractionation during the formation of liquid clouds, and both non-equilibrium and equilibrium fractionation during the formation of ice clouds (using the predicted super-saturation) as well as the re-evaporation of rain drops. For the parameterisation of moist convection, all physical processes during simulated convective up- and downdrafts affect the heavy isotopes in a similar way as the standard light humidity, again taking into account equilibrium and non-equilibrium fractionation when appropriate."

16. P6, L11: please add some details about this model. Does it run operationally? Is it an analysis? Does it run only for specific cases?

The IsoGSM global simulation data is constrained to reanalysis data with the help of a nudging technique. The Scripps Experimental Climate Prediction Center's GSM was based on the medium range forecast model used at NCEP for making operational analysis and predictions. Isotope ratios in water vapour with a spectral resolution of T62 and on 17 vertical levels are obtained from the IsoGSM simulation. This information has been included in manuscript.

♣ Page 6, from line 25

"[…] For the water isotopes, initial and boundary data are taken from a historical isotope global circulation model IsoGSM (which is based on the Scripps Experimental Climate Prediction Center's GSM that was used operationally for medium range forecasts at NCEP) simulation by Yoshimura et al. (2008), who performed these simulations using a nudging technique (see also Pfahl et al., 2012). The Scripps Experimental Climate Prediction Center's GSM was based on the medium range forecast model used at NCEP for making operational analysis and predictions."

17. P6, L12-16: Why is a resolution of 7 km used? Is this to be able to differentiate between convective and other precipitation by using the convection scheme's precipitation? Resources? Other reasons? Please specify.

This resolution was used for operational predictions at the German Weather Service DWD for a long time, such that the model is very well tuned in this configuration. We also chose this relatively coarse resolution because it allows for a large model domain that reduces the dependence on the much coarser isotope boundary data (spectral resolution of T62 in IsoGSM) and enables us to calculate backward trajectories consistently over longer periods.

♣ Page 16, from line 14

"[…] In this study, COSMOiso simulation at a horizontal grid spacing of about 7 km with parameterized convection results from a trade-off between having high enough resolution for including detailed dynamics of the mesoscale systems and being able to run efficiently over a large domain (about 4300 km × 3500 km) that includes the moisture plume over North Africa. This setup allows addressing the question we are interested in, namely: which isotope signals are due to local processes, and which are due to large-scale advection? To further study the details of the fractionation processes in and around deep convective systems, complementary investigations will be conducted using higher resolution convection-permitting simulation with a 2 km grid to shed a light on cloud microphysical processes inside deep convection."

18. P6, L22: 5 days trajectories in a 5 day simulation? So just back to the start of the simulation or until they leave the domain?

The trajectories are computed back in time until they leave the domain. The sentence has been corrected for sake of the readability.

♣ Page 7, line 12-13

"[…] The trajectories are computed five days back in time. Note that generally the COSMO trajectories move out of the regional model domain after 3 days."

19. P7, L6-8: Why are these values chosen?

The values are chosen based on the near sea surface temperature of SI region.

20. P7, L20: Spell out *two* in the section title

Corrected.

21. P7, L23: hour is abbreviated with just *h*

Corrected also at other places.

22. Fig.1: Some dots have edges, others have none. Remove all edges and make sure the higher precipitation measurements are plotted on top of the lower values to keep them clearly visible and not hide maxima. The Figure is very small and the comparison is difficult to read. In Fig. 1b all contour colors from 5 to 25 mm look almost exactly the same in print, please use a color table which shows the differences more clearly. Fewer levels might help to achieve better contrast, do you really need 24 different ones?

As suggested the edges have been removed and the size of color dots has been enlarged, and the color scale has been adjusted for sake of readability.

♣ Page 23

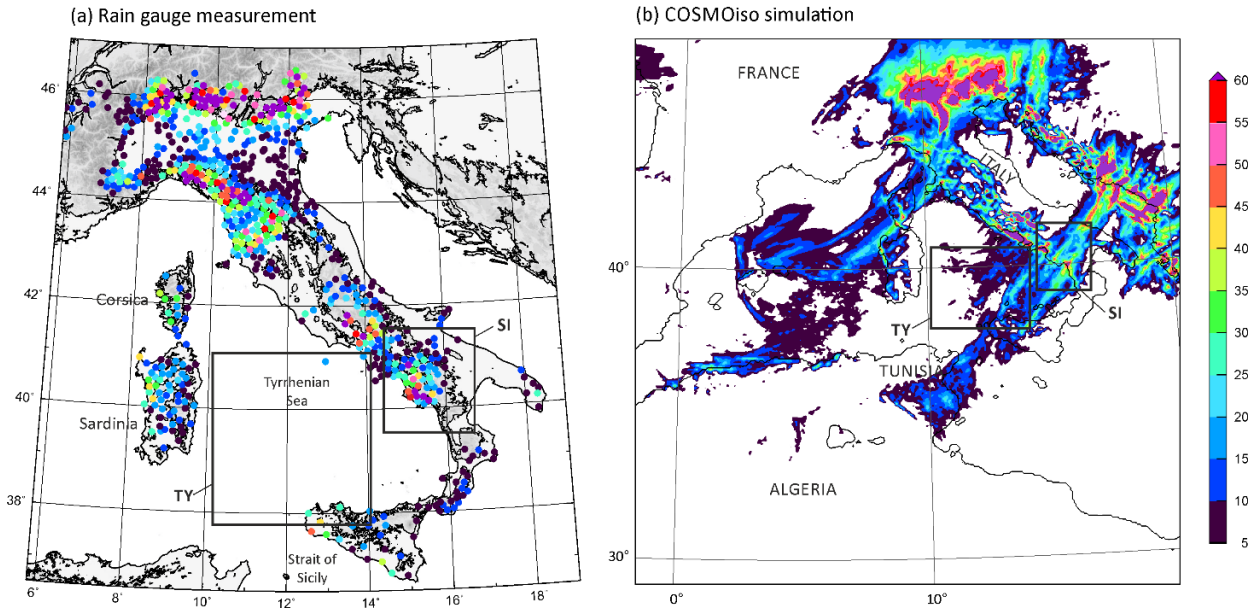

Figure 1. Accumulated precipitation during IOP 13 from 00 UTC on 15 October 2012 to 03 UTC on 16 October 2012 obtained from (a) rain gauge network, and (b) COSMOiso simulation.

23. P7, L26: *a large precipitation* rephrase
The sentence has been rephrased.

♣ Page 8, line 17
"shows precipitation in excess of 10 mm […]"

24. P7, L24-27: This sentence is too long and convoluted, simplify by moving the total precipitation amount to a separate sentence.
This sentence has been divided into two sentences.

♣ Page 8, line 15-20
"[…] The temporal evolution of the COSMOiso domain-averaged total precipitation within the SI area (bars in Figure 2) shows precipitation in excess of 10 mm within SI between 19 UTC on 15 October and 01 UTC on 16 October. The period has two distinct precipitation phases: 1) a convective precipitation phase (**P1**) in the late afternoon (19–21 UTC) on 15 October (dashed line in Fig. 2), and 2) a large-scale precipitation phase (**P2**) just before midnight (22–00 UTC) on that day (solid line). […]"

25. P8, L8: remove comma after *France*
Corrected.

26. Fig. 3: Change the colored contours of MSLP to lines, chose a good interval (not too dense) and smooth the field a bit if necessary. Add colored contours of 500 hPa geopotential to show the position of the trough. Move the vectors from the left panels to the right panes, they contain information of the same level.
The 500 hPa geopotential height is contoured on the shaded area of MSLP in the left panels of Figure 3.

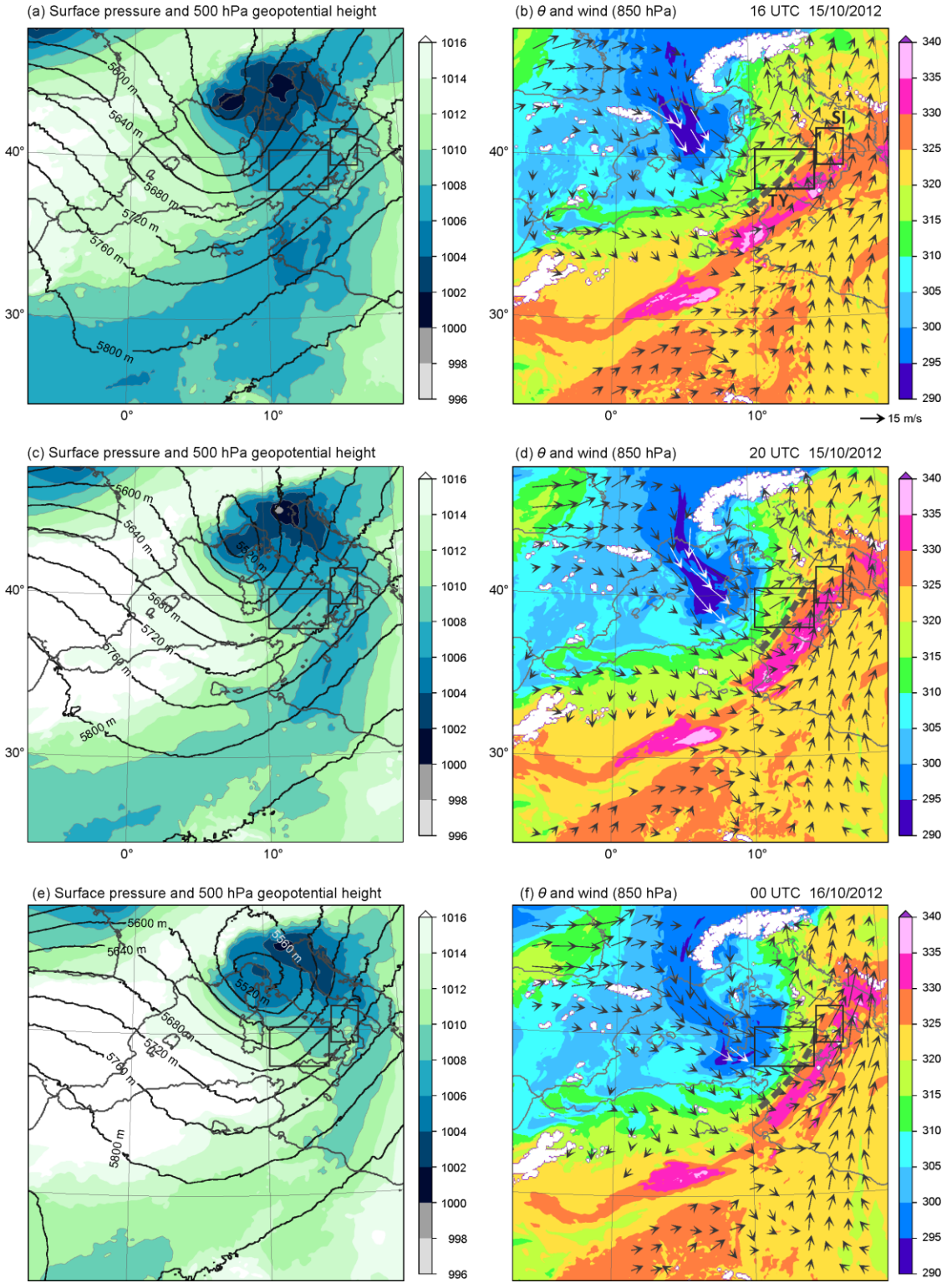

Figure 3. Horizontal distributions of sea level pressure (shades) and geopotential height at 500 hPa (contour) (left), and potential temperature, ϑ (shades), and wind (black and white arrows) at 850 hPa (right) at 16 UTC (top) and at 20 UTC (middle) 15 October 2012, and 00 UTC on 16 October 2012 (bottom) produced by the COSMOiso simulation. Coastal line is depicted by black line. The location of cold front is depicted by a dashed line in right panels.

27. P8, L11, 12: don't use *very* in scientific text, be specific.
Corrected.

♣ Page 9, line 10-15
"[…] winds associated with cold and dry air, with $\delta^{18}O_v$ less than –16‰ and q less than 2 g kg^{-1} (Fig. 4a, b), and thus low potential temperature, ϑ, are located over the Gulf of Lion (≤ 302 K, dark-blue area in Fig. 3b). […] the African moist plume with values of $\vartheta \geq 330$ K […]"

28. P8, L13: change *high ϑ values (≥ 330 K)* to *values of $\vartheta \geq 330$ K*
Corrected.

29. P8, L16, 17: Could convection be causing the cool areas in the 850 hPa potential temperature map over TY?
The original sentence was "Over the Tyrrhenian Sea ('TY' box in Fig. 1b), upstream of SI, a large horizontal ϑ gradient (315–330 K) can be seen at 850 hPa, indicating the elongation of the surface cold front along a southwest to northeast axis".
The convection positioned at the southern edge of this front, where high values of ϑ (≥ 325 K) are seen.

30. P8, L17: It is never explained that the model does, in fact, not produce two peaks. They are only visible when separating precipitation from the convection scheme and precipitation produced by microphysics.
The model, in contrast to the observations, does not produce two peaks in the total precipitation. These peaks can be seen by looking at the two precipitation types separately. This criticism has been included in manuscript.

♣ Page 8, line 24-26
"[…] P1 is related to rain from the convection parameterization, and P2 is related to rain associated with large-scale vertical motion. The model, in contrast to the observation, does not produce two peaks in the total precipitation. These peaks can be seen by looking at the two precipitation types separately."

31. P8, L18: the trough is never shown, add reference to Fig. 3 after adding the 500 hPa geopotential as suggested.
In the left panels of Figure 3, the 500 hPa geopotential height is contoured on the shaded area of MSLP. Please see the answer for comment #26.

32. P8, L23: *strong cyclonic flow* there is only one arrow within the box, curvature is hard to see.
The Figure 3 (right panels) has been corrected to see better the cyclonic flow, but very weak wind at the core region is not displayed for sake of readability.

33. P9, L12, 13: *very low* and *large* are not helpful in this context, just use the values. However, a short explanation on why the threshold between these two values is important would be helpful.
Corrected.

♣ Page 9, lines 10 and 16
"[…] cold and dry air, with $\delta^{18}O_v$ values less than −16 ‰ […]$\delta^{18}O_v$ values in excess of −25 ‰ can be seen […]"

34. P9, L26: the front is not really close to SI
The cold front is indicated where potential temperature (ϑ) values show a large gradient (315–330 K) at 850 hPa and it is marked by a dashed line in right panels of Fig. 3. We can see the front is close to SI.

35. P10, L27: *mostly very dry* use values instead, be specific
Corrected.

♣ Page 11, line 15-16
"[…] These air parcels are mostly dry ($q \leq 5$ g kg^{-1}) along the track during the 3 days […]"

36. P11, L2: remove *the* before q and $\delta^{18}O_v$, remove *values* after $\delta^{18}O_v$
Corrected.

37. P11, L6: change to *The median q value (…) factor of 2.5*
Corrected.

38. Fig 7: Figure has lots of white space and the way the map is shown causes even more. Try to reduce this to make the important parts a bit larger.
We have reduced much of white space and enlarged the figure.

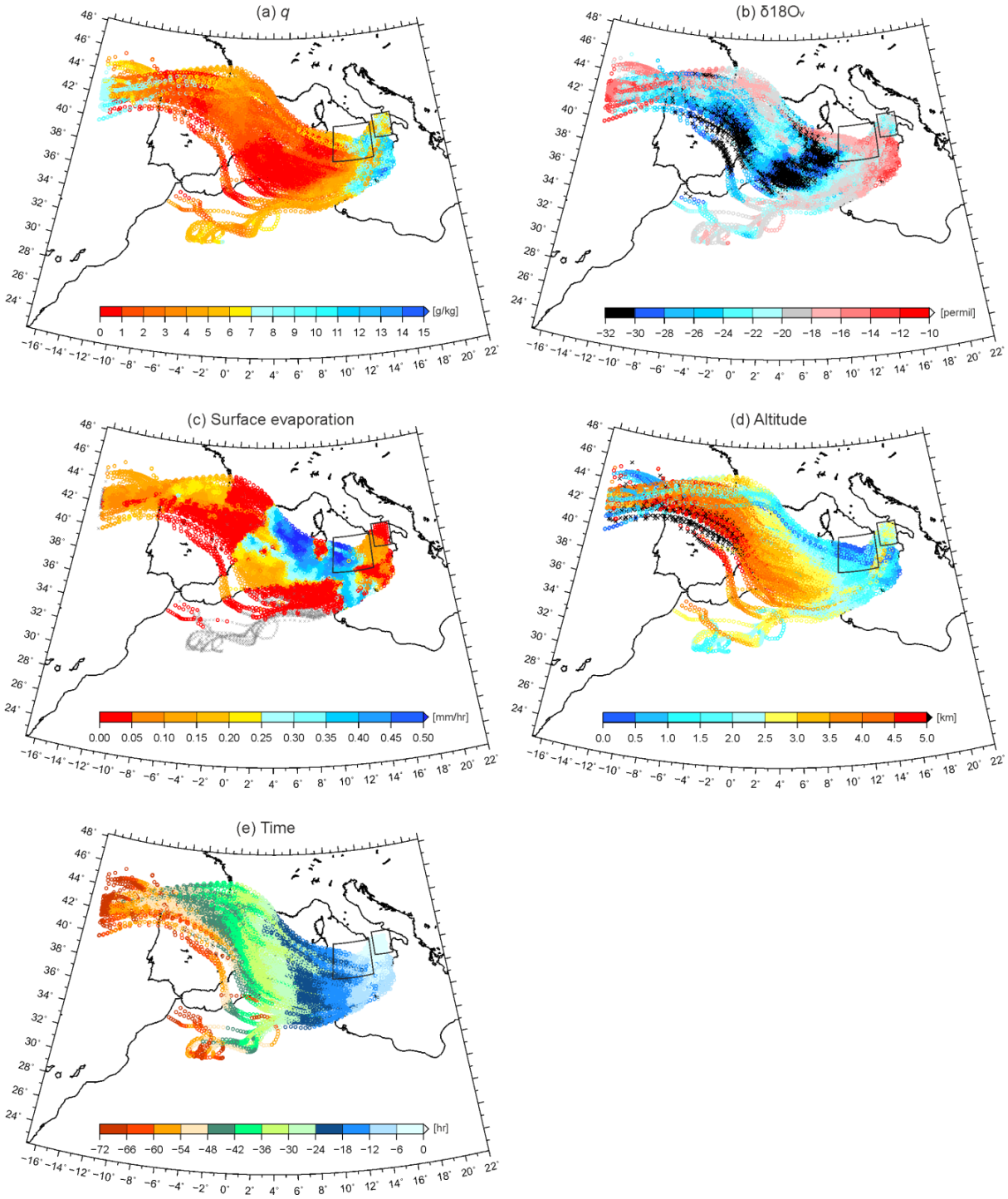

Figure 7. History of air parcel arriving at **SI** in layer of 800−700 hPa at 20 UTC on 15 October 2012. (a) water vapour mixing ratio, q (g kg^{-1}), (b) $\delta^{18}O_v$ (‰), (c) surface evaporation (mm h^{-1}), (d) altitude (km), and (e) time (h).

39. P11, L12: replace *the average q* with *q is about* 9 g kg^{-1} *on average*

Corrected.

40. P11, L14: It is never explained what a Rayleigh line is
Corrected.

41. P11, L19-21: This sentence is complicated. Also why?
The sentence was "This shows that the descending air parcels mix with the air parcels from lower altitudes, and near surface air parcels mix between surface evaporation and background vapour".
Figure 9a, b show that the lower to upper-level trajectories (0.1–7 km altitudes) follow a mixing line during their descent, and this indicates that the descending air parcels from upper levels mix with the air parcels from lower altitudes. The descent of drier air parcel to near the sea surface also increases evaporation. For sake of clarity, this sentence has been improved.

♣ Page 12, line 8-9
"[…] This shows that the descending dry air parcels mix with the warm and moist air parcels from lower altitudes, which also increases surface evaporation."

42. P11, L28: replace *many* with *multiple*, change *convection* to *convective*
Corrected.

43. P12, L2: usage of low/high seems inconsistent looking at the numbers
The sentence has been rewritten.

♣ Page 12, line 18-19
"[…] Within the precipitation area, relatively lower $\delta^{18}O_v$ values (≤ −16 ‰) than in the vicinity are found at 542 m ASL while relatively high $\delta^{18}O_v$ values between −20 and −24 ‰ are found at 2455 m and 5565 m ASL […]"

44. P12, L13: change to *with values of* $\delta^{18}O_v$ *larger than;* replace *toward* with *around*
Corrected.

45. P12, L18-19: rewrite sentence
Corrected.

♣ Page 13, line 7-8
"The Lagrangian analysis indicates that most of the processes inducing precipitation during P1 take place during the last 18 hours over the Tyrrhenian Sea and the Strait of Sicily."

46. P12, L25: change to *convective mixing injects SWI-enriched moisture into higher altitudes*
Corrected.

47. Fig. 8: explain colors in the caption, some dots have edges and others don't, figure is small, you could change the aspect ratio to fit the page width for better readability. This also applies to the other figures of this type (9 and 12).
As suggested the Figure 8 has been improved for better readability. However we kindly propose to keep the aspect ratio of the figure to better identify the characteristics.

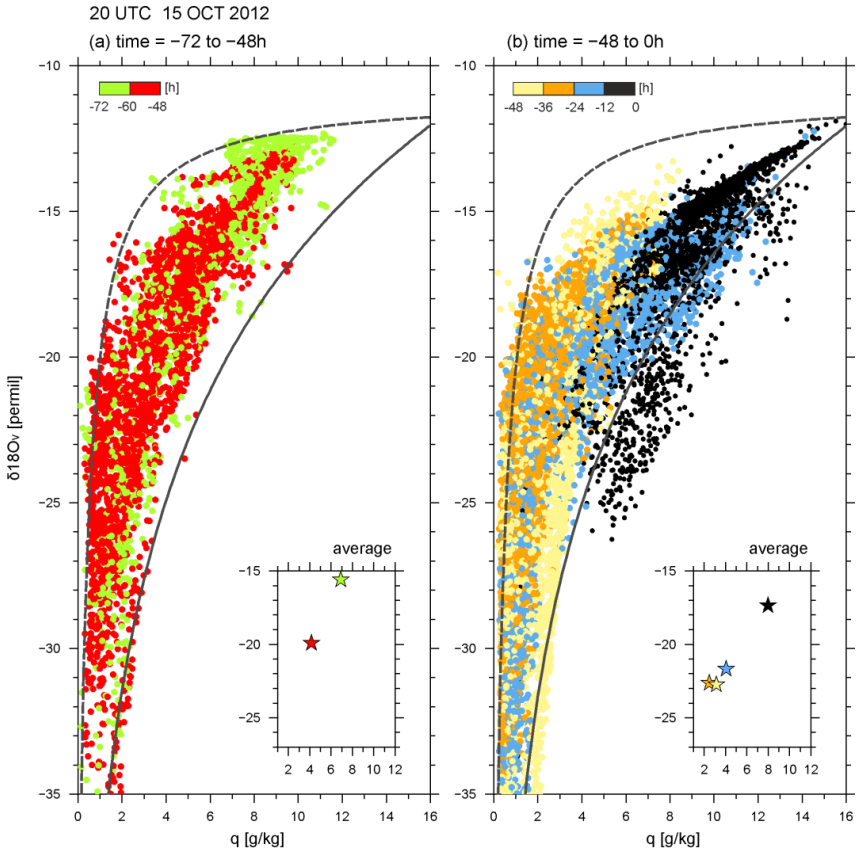

Figure 8. Scatter diagram of q and $\delta^{18}O_v$ along the backward trajectories of Figure 7 during (a) the times between −72 and −48 h, and (b) times between −48 and 0 h every 12 hours from 20 UTC on 15 October 2012. The colour of dot changes every 12 h. The mixing and Rayleigh lines are indicated in each panel by dashed and solid line, respectively. The averaged q and $\delta^{18}O_v$ every 12 hours is displayed in the bottom right corner of each panel.

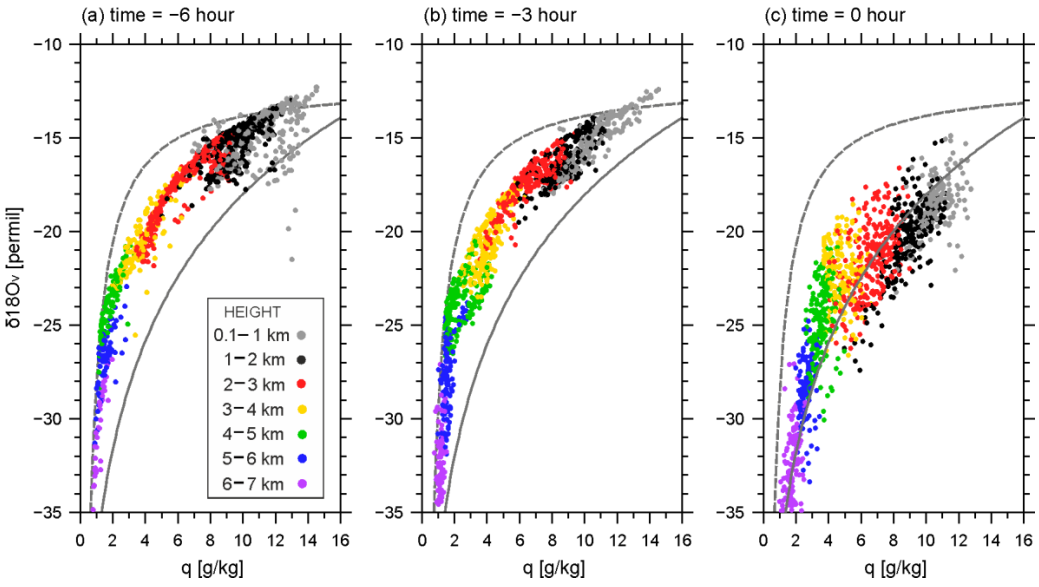

Figure 9. Scatter diagram of q and $\delta^{18}O_v$ along the backward trajectories of Figure 7 but for all altitudes of 1–2 km (black dots), 2–3 km (red dots), 3–4 km (yellow dots), 4–5 km (green dots), 5–6 km (blue dots), and 6–7 km (purple dots) at (a)

−6 h, (b) −3 h, and (c) 0 h from 20 UTC on 15 October 2012. The mixing and Rayleigh lines are indicated in each panel by dashed and solid line, respectively.

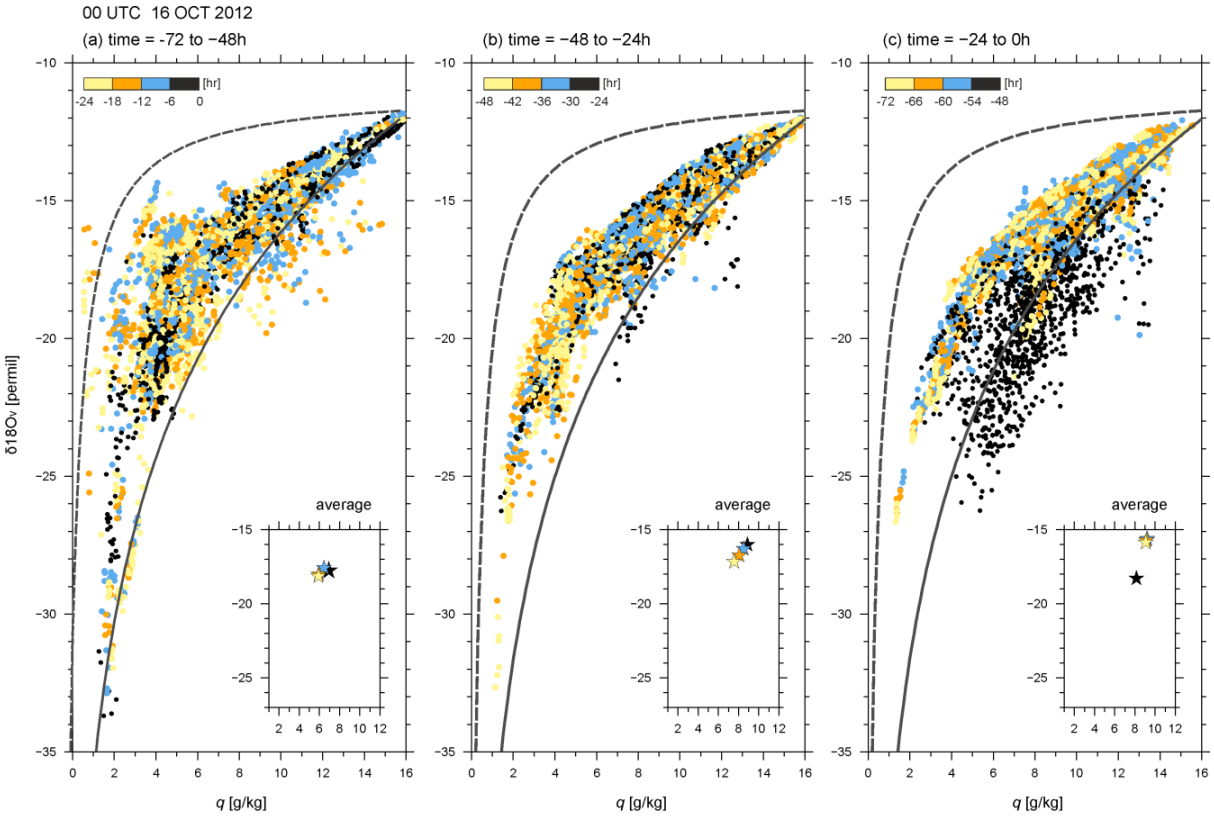

Figure 12. Scatter diagram of q and $\delta^{18}O_v$ along the backward trajectories of Figure 11 during (a) the times between −72 and −48 h, (b) times between −48 h and −24 h, and (c) times between −24 h and 0 h from 00 UTC on 16 October 2012 every 6 hours. The colour of dot changes every 6 h. The mixing and Rayleigh lines are indicated by dashed and solid line, respectively. The averaged q and $\delta^{18}O_v$ every 6 hours is displayed in the bottom right corner of each panel.

48. Fig. 10: panel titles say *vapour* and *rain water*, change them to clearly indicate that they show $\delta^{18}O_v$ **for** vapour/rain water. Also, model levels are not at a constant height. Does this have any effect over mountains? If so, explain which one? Better alternative: plots for certain altitudes above sea level, e.g. 500, 2500, and 5000 m, instead of model levels.

The panel titles have been corrected to $\delta^{18}O_v$, $\delta^{18}O_r$, and $\delta^{18}O_s$ correspondingly. The figure 10 shows $\delta^{18}O_v$, $\delta^{18}O_r$, and $\delta^{18}O_s$ at a model level 8, 16, and 23 which altitudes are about 542 m, 2455 m, and 5565 m above the sea surface, respectively, in regions without topography. However, as noted by the reviewer, the model levels follow the terrain and the fields are thus shown for different altitudes over topography. As the precipitation in SI region occurred mostly near the coast, and the associated moisture processes occurred over the Tyrrhenian Sea and Strait of Sicily, we keep the plot as it is, but a note has been added to the caption.

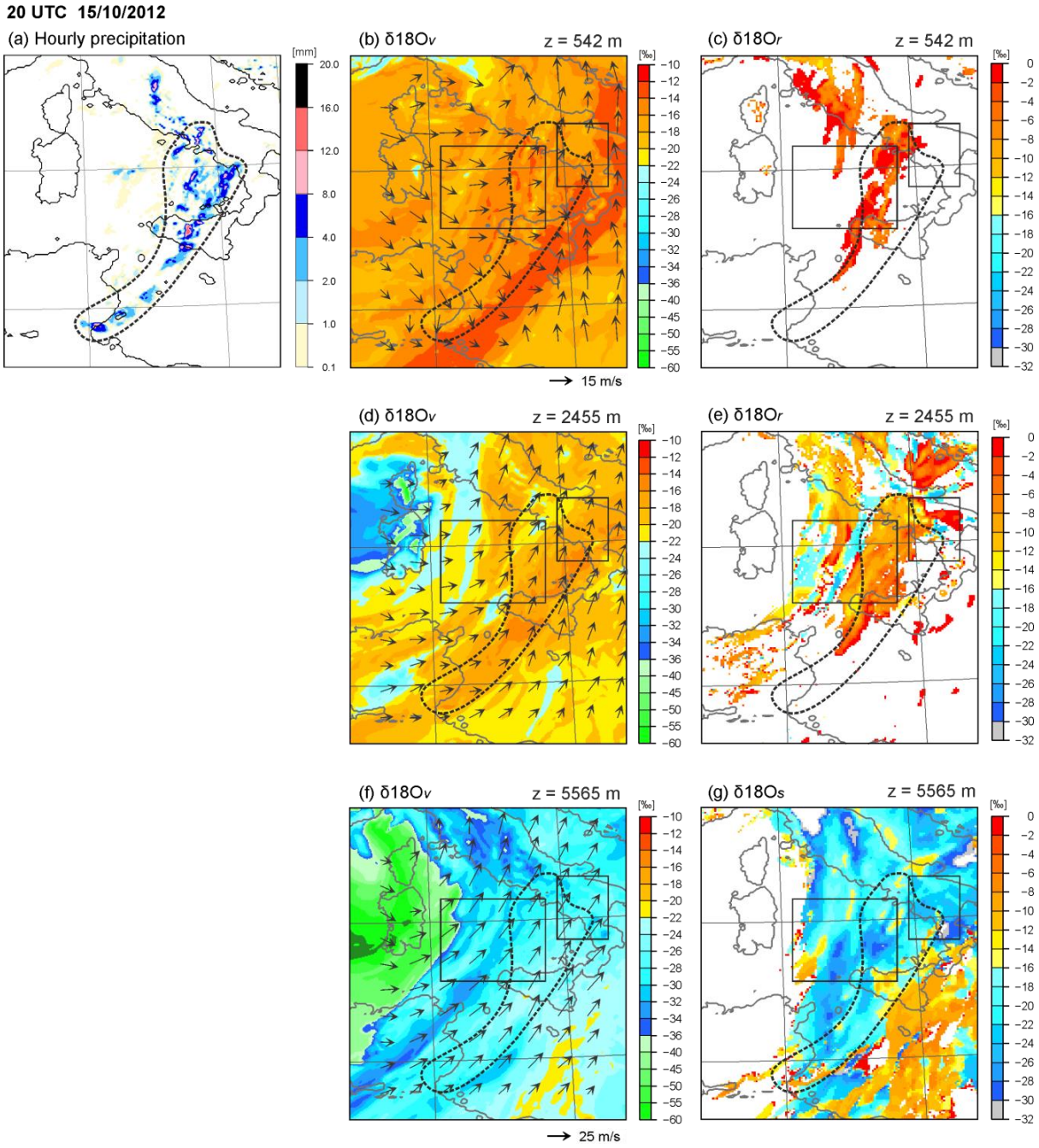

Figure 10. Horizontal distributions of (a) surface hourly precipitation (mm), $\delta^{18}O_v$ (‰) at (b) model level 8 (about 542 m ASL), (c) model level 16 (about 2455 m ASL), and (d) model level 23 (about 5565 m ASL, $\delta^{18}O_r$ (‰) at (e) 542 m ASL and (f) 2455 m ASL, and $\delta^{18}O_s$ (‰) at 5565 m ASL at 20 UTC on 15 October 2012. Note that, due to the terrain-following coordinates, the SWI values are partly depleted over topography, e.g. in central Italy. The precipitating area is marked by the area enclosed by the dashed line.

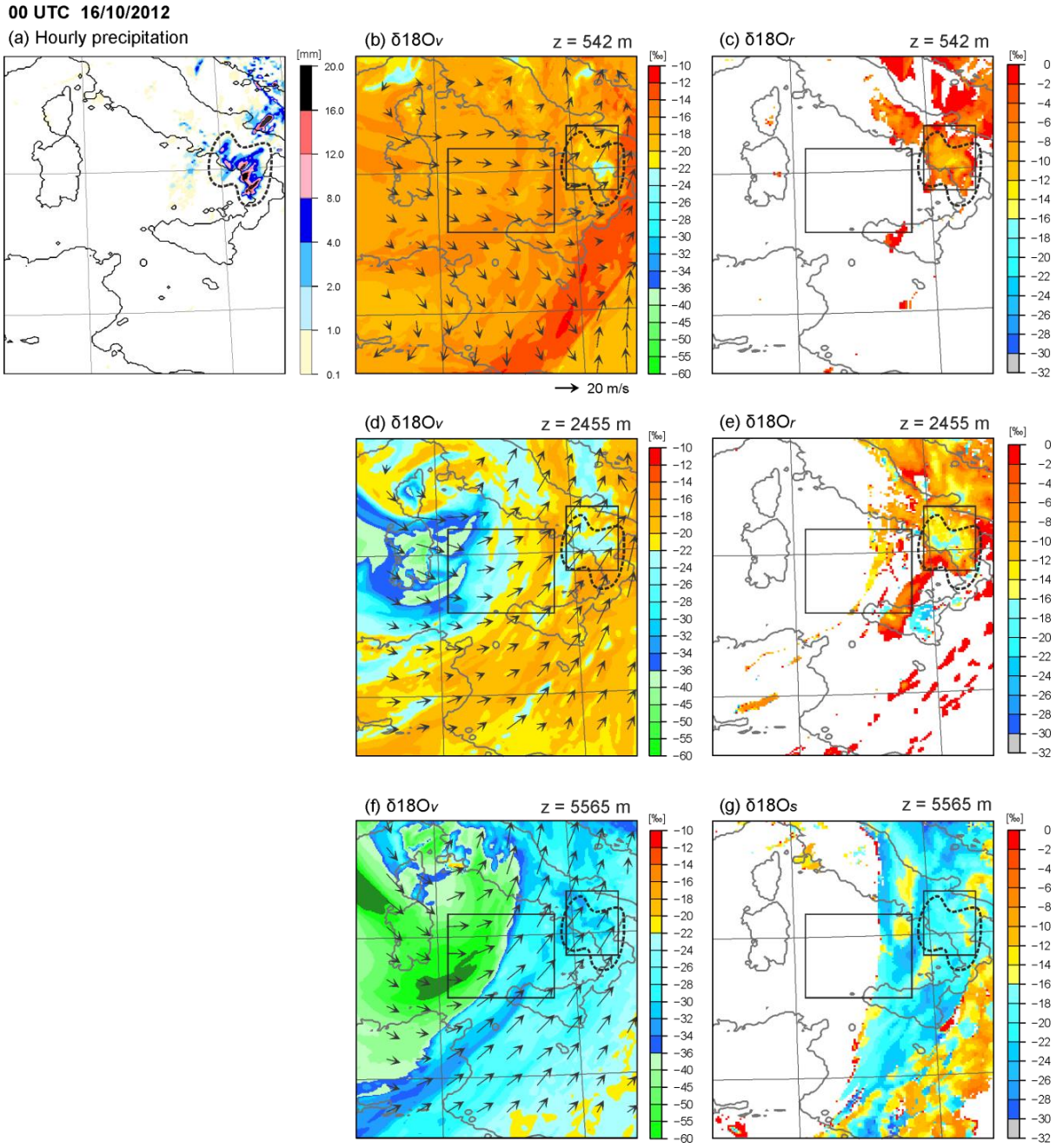

Figure 13. Same as Figure 10 but for 00 UTC on 16 October 2012.

49. P13, L2: replace *over* with *from*

Corrected.

50. P13, L3: Threshold of 5 g kg^{-1} is not visible in the figure

The value is obtained from an average over all trajectories, not those shown in Figure 11. For better understanding, the sentence has been corrected.

♣ Page 13, line 20-21
"The air parcels are consistently moist along the tracks (Fig. 11a), with average *q* value mostly ≥ 5 g kg^{-1} along the track, in contrast […]"

51. P13, L7: replace *for instance* with *and*
Corrected.

52. P13, L7, 8: Use a non-breaking space between multiple units, in LaTeX to avoid line breaks between them. This can be done by using ~ instead of a pace like this: 9~g~kg or in MS word by using Ctrl + Shift + Space
We appreciate the guide. The non-breaking space has been used entire manuscript.

53. P13, L20-21: rephrase, also, do not use *precipitation cell* unless explicitly referring to a single convective cell
Corrected.

♣ Page 14, line 8-10
"At 00 UTC on 16 Oct. during P2, stronger precipitation than that of P1 is produced, and the precipitation system is located mainly over SI (marked area closed by dashed line in Fig. 13a). In the vicinity of the precipitating region, strong cyclonic south-westerly flow ≥ 25 m s^{-1} is dominant at 2455 m and 5565 m ASL (Fig. 13d, f)."

54. P13, L24: The depletion is hardly visible at 5500 m
The depletion at 5565 m is visible with the improved color scale of Figure 13.

55. P14, L1-5: going back to earlier Figures is tedious and disrupting, try to avoid if possible by restructuring the text
Agreed. However we kindly propose to keep as it is to complete our comprehension from entire analysis.

56. P14, L6-8: rephrase sentence
Corrected.

♣ Page 14, line 24-25
"The Lagrangian analysis indicates that the moistures that feeds the convection during P2 is coming from North Africa and the air parcels take up additional moisture (2–3 g kg^{-1}) over the Mediterranean."

57. P14, L9: replace *entrainment* with *mixing,* entrainment is usually used in the context of convective updrafts
Corrected.

58. P14, L15: replace *convective* with *convection*
Corrected.

59. P14, L20: the three paragraphs starting here are especially long and too descriptive, be more concise. Do not simply repeat details from previous sections in the conclusions.
The three paragraphs become concise by removing the repeated description.

60. P15, L4, 5: do not use formulations like *totally different* in scientific texts
Corrected to "arriving at SI is *distinct*".

Contrasting stable water isotope signals from convective and large-scale precipitation phases of a heavy precipitation event in Southern Italy during HyMeX IOP 13: a modelling perspective

Keun-Ok Lee[1], Franziska Aemisegger[2], Stephan Pfahl[2,3], Cyrille Flamant[4], Jean-Lionel Lacour[5], and Jean-Pierre Chaboureau[1]

[1]Laboratoire d'Aérologie, Université de Toulouse, CNRS, UPS, Toulouse, France

[2]Institute for Atmospheric and Climate Science, ETH Zurich, 8092 Zurich, Switzerland

[3]Institute of Meteorology, Freie Universität Berlin, Berlin, Germany

[4]LATMOS/IPSL, CNRS, Sorbonne Université and Université Paris-Saclay, Paris, France

[5]Institute of Earth Sciences, University of Iceland, Reykjavik, Iceland

ABSTRACT

The dynamical context and moisture transport pathways embedded in large scale flow and associated with a heavy precipitation event (HPE) in Southern Italy (SI) are investigated with the help of stable water isotopes (SWIs) based on a purely numerical framework. The event occurred during the intensive observation period (IOP) 13 of the field campaign of the Hydrological Cycle in the Mediterranean Experiment (HyMeX) on 15 and 16 October 2012 and SI experienced intense rainfall of 62.4 mm over 27 h with two precipitation phases during this event. The first one (P1) was induced by convective precipitation linked to a frontal feature, while the second one (P2) was mainly associated with precipitation induced by large-scale uplift. The moisture transport and processes responsible for the HPE are analysed using a simulation with the isotope-enabled regional numerical model $COSMO_{iso}$. Backward trajectory analyses based on this simulation show that the air parcels arriving in SI during P1 originate from the North Atlantic, and descend within an upper-level trough over the north-western Mediterranean. The descending air parcels reach elevations below 1 km over the sea and bring dry and isotopically depleted air (median $\delta^{18}O \leq -25$ ‰, water vapour mixing ratio $q \leq 2$ g kg^{-1})

close to the surface, which induces strong surface evaporation. These air parcels are rapidly enriched in SWI ($\delta^{18}O \geq -14$ ‰) and moistened ($q \geq 8$ g kg^{-1}) over the Tyrrhenian Sea by taking up moisture from surface evaporation and potentially from evaporation of frontal precipitation. Thereafter, the SWI-enriched low-level air masses arriving upstream of SI are convectively pumped to higher altitudes, and the SWI-depleted moisture from higher levels is transported towards the surface within the downdrafts ahead of the cold front over SI, producing a large amount of precipitation of convective nature in SI. Most of the moist processes (i.e. evaporation, convective mixing) related to the HPE take place during the 18 hours preceding the occurrence of P1 over SI. Four hours later, during the second precipitation phase P2, the air parcels arriving over SI mainly originate from North Africa. The strong cyclonic flow around the eastward moving upper-level trough induces the advection of a moist and SWI-enriched African plume towards SI, and leads to large-scale uplift of the warm African air mass along the cold front. This brings moist and SWI-enriched air masses (median $\delta^{18}O \geq -16$ ‰, median $q \geq 6$ g kg^{-1}) to higher altitudes and leads to gradual rain out of the air parcels over Italy. Large-scale ascent in the warm sector ahead of the cold front takes place during the 72 hours preceding P2 in SI. This work demonstrates how stable water isotopes can yield additional insights into ~~sheds light on~~ the variety of thermodynamic mechanisms occurring at the meso- and synoptic scales during the formation ~~and leading to two distinct precipitation phases~~ of a HPE ~~over the densely populated SI region~~.

1. Introduction

The Mediterranean basin is frequently affected by deep convection resulting in heavy precipitation and potentially leading to devastating flash floods. Deep convection generally results from complex multi-scale interactions between large-scale, mesoscale, and microphysical processes. In the north-western Mediterranean, the large-scale patterns associated with heavy precipitation events (HPEs) have been shown to be connected to upper-level troughs, responsible for generating low-level northward flow of marine air masses characterized by high values of equivalent potential temperature and precipitable water (Lin et al., 2001; Martius et al., 2006; Nuissier et al., 2008, 2011; Ricard et al., 2012; Barthlott and Davolio, 2015). In this favourable large-scale situation, mesoscale deep convection can occur and often produces high-impact events, along with rainfall amounts larger than 100 mm in less than 6 hours. The origin of the moisture content feeding the deep

convective systems is an important question that has been addressed using different techniques and tools, such as trajectory and numerical tracer analyses (*e.g.* Turato et al. 2004; Winschall et al., 2012; Duffourg and Ducrocq, 2013; Winschall et al., 2014; Röhner et al., 2016; Duffourg et al., 2018; Lee et al., 2018). These studies found substantial contributions of subtropical and tropical moisture coming either from Africa (latitude ≥ 20°N) or from the extratropical remnants of Atlantic tropical cyclones. More recent studies (*e.g.* Lee et al. 2016 and 2017) pointed out the intrusion of large moisture, e.g. ~~amounts~~one quarter of total integrated water vapour, from North Africa in the mid-troposphere (3-5 km above sea level, ASL) feeding the deep convective systems together with the local water vapour sources over the Mediterranean in the lower troposphere (below 2 km ASL). Moreover, the importance of intensified evaporation over the Mediterranean Sea surface for HPE has been studied (Duffourg and Ducrocq, 2013; Winschall et al., 2014). The vertical distribution of moisture in the atmosphere is shaped by source, transport, and sink processes, e.g. evaporation and condensation, horizontal and vertical advection, as well as turbulent and convective mixing.

To improve our understanding of the water vapour transport upstream of HPEs and the moisture cycling during such events, humidity observations based on measurements of the most abundant stable water isotopes (SWI) $H_2{}^{16}O$ alone can be limited. In this context, the SWI observation of other, less abundant SWIs, i.e. $H_2{}^{18}O$ and $HD^{16}O$ can provide relevant additional constrains (Noone et al., 2012; Pfahl et al., 2012; Aemisegger et al. 2015; Galewsky et al., 2016; Sodemann et al., 2017). Heavy and light isotopes of the water molecule are partitioned in a very specific way during phase transitions, leading to an enrichment of the heavier molecules compared to the lighter ones in the phase with the stronger bonds (liquid or ice) and a depletion in ~~the other phase (~~vapour~~)~~. Therefore, they can provide a record of evaporation and condensation ~~processes~~ cycles during the transport of air parcels. Since the strength of fractionation depends on the meteorological conditions (temperature and the level of saturation), SWI are a powerful indicator of phase change conditions in the atmosphere that occur during the transport of air parcels on a broad range of scales, reflecting evaporation, condensation, and air mass mixing processes (e.g., Sodemann et al., 2017). For instance, low δ^2H (typical range between –160 and –180 ‰) or $\delta^{18}O$ (i.e. range between –20 and –30 ‰) values in atmospheric water vapour at surface ~~($\delta^{18}O = (Rs/RVSMOW - 1) \times 1000$, where $Rs = [H_2{}^{18}O]/[H_2{}^{16}O]$ is the isotope ratio of a water sample and RVSMOW is the isotope ratio of the Vienna Standard Mean Ocean Water)~~ indicate ~~the origin of~~

low air mass temperatures and strong rainout of air parcels (e.g. Jacob and Sonntag, 1991; Yoshimura et al., 2010), whereas high δ^2H (typical range between –120 and –100 ‰) or $\delta^{18}O$ (range between –18 and –14 ‰) indicate high air mass temperatures and recent admixture of fresh ocean evaporate. The δ notation describes the concentrations of the heavy isotopes relative to the isotope ratio of the Vienna Standard Mean Ocean Water–RVSMOW, by for instance, $\delta^{18}O = (Rs/RVSMOW - 1) \times 1000$, where $Rs = [H_2{}^{18}O]/[H_2{}^{16}O]$ is the isotope ratio of a water sample.

In the past, some of the most prominent applications of SWIs have been in a paleoclimate context to infer past temperatures and moisture sources from natural archives, for groundwater studies, and in studies investigating the water vapour budget in the stratosphere (Sherwood and Dessler, 2000; Vimeux et al., 2001; Dessler and Sherwood, 2003; Jouzel et al., 2005). The process-based insight provided by the isotope composition of atmospheric water~~,~~ have more recently been extended to synoptic and sub-diurnal timescales~~,~~ and to the lower troposphere, where most atmospheric water vapour resides. Thanks to a tremendous expansion in the number of datasets of water vapour isotopic composition and a substantially improved set of theories and models for interpreting them, the related studies have been expanded during the past several years (*e.g.* Pfahl et al. 2008; Steen-Larsen et al. 2014; Bonne et al. 2014; Aemisegger et al. 2015; Dütsch et al., 2017; Lacour et al., 2017; Christner et al., 2018).

Recent studies have shown the unique information about meteorological processes registered in SWI data. For instance, using ground-based SWI measurements and numerical simulations, Pfahl et al. (2012) and Aemisegger et al. (2015) investigated the mixing processes of different air masses, as well as isotope fractionation and equilibration in relationship with precipitation evaporation, during the passage of cold fronts. Aemisegger and Papritz (2018) and Aemisegger and Sjolte (2018) showed that the important moisture uptake by cold and dry airstreams during events of strong large-scale ocean evaporation carries a distinct SWI-signature in water vapour. Recent studies (Schneider et al. 2016; Lacour et al. 2017) analysed the influence of the Saharan heat low on the isotopic budget of the free troposphere offshore of West Africa on various temporal and spatial scales, highlighting the importance of the Saharan heat low dynamics on the moistening and the SWI enrichment of air parcels in the free troposphere over the North Atlantic. In addition, Risi et al. (2008) used stable isotopic signals to better understand convective precipitation processes. These previous studies

evidenced the usefulness of water vapour isotope data to better understand meteorological processes and moisture transport. Nevertheless, there are still very few studies (Risi et al., 2008 and 2010; Tremoy et al., 2014) focusing on the application of water vapour isotopes to investigate moist processes associated with HPEs at the mesoscale, particularly in the extratropics.

SWI measurements are mainly obtained from space-borne retrievals (e.g. Schneider et al., 2016; Lacour et al., 2017) and ground-based in-situ laser spectroscopy (e.g. Aemisegger et al., 2012). The space-borne measurements provide continuous datasets in space at the global scale with coarse vertical resolution and limited precision. On the other hand, ground-based measurements with high temporal resolution are only available from a few locations and from dedicated field campaigns. In particular, the data availability for the Mediterranean region is very limited. A notable exception is the airborne dataset acquired around Corsica (Sodemann et al., 2017) during the first Special Observing Period of the Hydrological cycle in the Mediterranean Experiment (HyMeX SOP-1, Ducrocq et al., 2014). However, it does not include SWI observations for the days under scrutiny in this paper. Due to these limitations we use a model to demonstrate the usefulness of SWI data for understanding moist processes associated with a Mediterranean HPE.

Our study focuses on the transport of moisture associated with a HPE that occurred over southern Italy (SI) on 15−16 October 2012 and produced precipitation over land exceeding 60 mm in 27 h~~r~~ (Fig. 1a). The HPE consists of two precipitation peaks, the first peak in the late afternoon of 15 October and the second peak around midnight on that day. The target HPE occurred during the Intensive Observation Period 13 (IOP 13) of the HyMeX SOP-1. Using a combination of ground-based, airborne and space-borne observations and numerical simulations of this HPE, ~~that occurred during the Intensive Observation Period 13 (IOP 13) of the first Special Observing Period of the Hydrological cycle in the Mediterranean Experiment (HyMeX SOP-1, Ducrocq et al., 2012),~~ Lee et al. (2016) investigated the detailed dynamic and thermodynamic environments of the two precipitation phases of the HPE. During Phase 1 (P1), rainfall was connected to convection triggered by local low-level convergence ahead of a cold front and was favoured by moist conditions in the low levels over the Tyrrhenian Sea. Heavy precipitation during Phase 2 (P2) was initiated over Algeria and was favoured by the southerly flow ahead of the upper-level trough and large low-level moisture content and high sea surface temperature in the Strait of Sicily. The penetration of the mistral ~~wind~~ over the Mediterranean and SI at the

end of 15 October terminated the convectiveon activity. Thanks to the unprecedented data acquired offshore and inland during IOP 13, the detailed moisture structure upstream of the HPE was investigated by Lee et al. (2016). They highlighted 1) the presence of an African moisture plume favouring the efficiency of the convection to produce more precipitation, 2) the importance of southerly flow from the warmer Mediterranean Sea south of Sicily in enhancing the convergence ahead of the cold front, and 3) the role of the upper-level trough over southern France extending to the western Mediterranean in organizing convection at the leading edge of the surface front. However, the moisture origin and the humidity transport pathways of moisture that are involved in the HPE over SI have not been studied to date.

Here we investigate these moisture transport processes using trajectory calculations and SWI data obtained from a numerical simulation with 7-km horizontal resolution. A detailed description of the data and methodology is presented in section 2. Section 3 provides an overview of the meteorological conditions during the two precipitation peaks related to the HPE during IOP 13. Section 4 discusses the isotope signals and relates them to the moisture transport history. A summary and a discussion of the findings of the present study are given in section 5.

2. Data and method

2.1. COSMOiso model configuration and simulation

The COSMO model (Steppeler et al., 2003) is a non-hydrostatic, limited-area numerical weather and climate prediction model and is operationally used by several European weather services. The isotope implementation (COSMOiso; Pfahl et al., 2012) is similar to other Eulerian isotope models (e.g. Joussaume et al., 1984; Sturm et al., 2005; Blossey et al., 2010). COSMOiso has already shown its capability to simulate the variations of stable water isotopes at the event-timescale (Pfahl et al., 2012; Aemisegger et al. 2015) as well as in a climatological sense (Christner et al. 2018; Dütsch et al. 2018). It includes two additional parallel water cycles for each of the heavy isotopes ($H_2{}^{18}O$, $HD^{16}O$), which are used purely diagnostically and do not affect other model components. All prognostic moisture fields, which are simulated by the model in terms of specific humidities, are duplicated twice, representing the specific humidities of $H_2{}^{18}O$ and $HD^{16}O$, respectively. From the prognostic specific humidity fields, the isotope ratios in usual δ-notation can be calculated. The heavy

isotopes experience the same processes as the light isotope ($H_2{}^{16}O$), except during phase transition, when isotopic fractionation occurs. A one-moment microphysics scheme is used and deep convection is parameterised following Tiedtke (1989). In the microphysical scheme, transfer rates between the different water species during the formation of clouds and precipitation are specified. The heavy isotopes are affected by equilibrium fractionation during the formation of liquid clouds, and both non-equilibrium and equilibrium fractionation during the formation of ice clouds (using the predicted super-saturation) as well as the re-evaporation of rain drops. For the parameterisation of moist convection, all physical processes during simulated convective up- and downdrafts affect the heavy isotopes in a similar way as the standard light humidity, again taking into account equilibrium and non-equilibrium fractionation when appropriate. For a detailed description of the physics and isotope parameterisations, see Doms et al. (2011) and Pfahl et al. (2012), respectively.

Operational analysis data from the European Centre for Medium-Range Weather Forecasts (ECMWF) are used as boundary and initial conditions for the standard model variables. For the period in October 2012, these data are available every six hours with a spectral resolution of T1279 and 91 vertical levels and are interpolated to the COSMO grid. After the model initialisation, information from the analysis data is only used at the model boundaries, employing a relaxation scheme following Davies (1976). For the water isotopes, initial and boundary data are taken from a historical isotope global circulation model IsoGSM (which is based on the Scripps Experimental Climate Prediction Center's GSM that was used operationally for medium range forecasts at NCEP) simulation by Yoshimura et al. (2008), who performed these simulations ~~employed the IsoGSM global model data~~ using a nudging technique (see also Pfahl et al., 2012). The Scripps Experimental Climate Prediction Center's GSM was based on the medium range forecast model used at NCEP for making operational analysis and predictions.

In this study, a horizontal grid spacing of 0.0625° (in a rotated grid), corresponding to approximately 7 km, and 40 hybrid vertical levels are used. The model domain covers the northwestern Mediterranean, the east Atlantic, and the northern African regions (longitude ranging from –16.3 to 22.8°E and latitude ranging from 17.3 to 49.2°N). The simulation starts at 00 UTC on 12 October 2012, and runs for 5 days producing output fields every hour.

2.2. Trajectory calculation

Air parcel backward trajectories (Wernli and Davies, 1997; Sprenger and Wernli, 2015) are calculated using the three-dimensional wind fields from the COSMOiso simulation. In total 1440 trajectories per hourly time step are started from 60 grid points within a box over SI (bounded by 15.2°W, 16.6°W, 39.6°N, 41.3°N; Fig. 1) and 24 different vertical levels between 1000 and 400 hPa. The trajectories are computed five days back in time. Note that ~~G~~generally~~, after 3 days~~ the COSMO trajectories move out of the regional model domain after 3 days. The air parcel position as well as the interpolated conditions ($\delta^{18}O$, water vapour mixing ratio -q, surface evaporation) along the trajectories are written as an output every hour. In this study, two series of trajectories, starting at the times of the two precipitation peaks (20 UTC on 15 October 2012 and 00 UTC on 16 October 2012; lines in Fig. 2) over SI are discussed.

2.3. $q-\delta$ analysis

As variations in δ are tied to those in humidity, q, the $q-\delta$ space is often used for the interpretation of the information contained in δ. The theoretical framework for interpreting paired $q-\delta$ data is based on a set of simple models that account for mixing and a range of condensation conditions (Noone, 2012). The isotopic depletion of water vapour that undergoes condensation at equilibrium can be described by a Rayleigh distillation model as $\delta = (\alpha-1) \ln (q/q_0) + \delta_0$, in which q_0 and δ_0 are the humidity and the isotopic composition of the water vapour source, and α is the coefficient of fractionation. In this study, q_0 and δ_0 are set to 15 g– kg^{-1} and −10 ‰, respectively. The mixing model is $\delta = q_0 (\delta_0 - \delta_F) 1/q + \delta_F$, in which the subscript F denotes the flux into the volume of interest, here set to −12 ‰.

Mixing and distillation of water vapour from different sources can occur over a wide range of combinations and produce $q-\delta$ pairs in between these two boundary models. A Rayleigh model with a tropical water vapour source can generally be used to describe the lower limit of the domain of existence of $q-\delta$ pairs. The upper limit of this domain can be described by a mixing model between depleted and dry air from the upper troposphere and enriched and humid air from the tropical boundary layer. The large-scale distribution of water vapour isotope ratio is conveniently viewed as a balance between the depleting effects of condensation

(such as in a Rayleigh processes), mixing of air masses with vapour of differing isotopic composition during large-scale transport and the enriching effects during supply from a boundary layer source (Noone 2008; Galewsky and Hurley 2010). Also note that raindrop re-evaporation can lead to q−δ pairs below the Rayleigh distillation model (Worden et al., 2007).

3. Overview of meteorological condition

3.1 One HPE with ~~2~~ two precipitation phases over southern Italy

From 00 UTC on 15 October to 03 UTC on 16 October 2012, the SI area (box marked by 'SI' in Figure 1) was affected by a HPE, with two phases of precipitation. The large amount of maximum precipitation (in total 62.4 mm over 27 h~~r~~) recorded by the rain gauge network (Fig.1a) is realistically reproduced by COSMOiso simulation (maximum precipitation of 59 mm, Fig. 1b) both in terms of amplitude and spatial distribution. The temporal evolution of the COSMOiso domain-averaged total precipitation within the SI area (bars in Figure 2) shows ~~a large~~ precipitation ~~within the SI~~ in excess of 10 mm within the SI between 19 UTC on 15 October and 01 UTC on 16 October~~.~~, The period has ~~with~~ two distinct precipitation phases: 1) a convective precipitation phase (**P1**) in the late afternoon (19−21 UTC) on 15 October (dashed line in Fig. 2), and 2) a large-scale precipitation phase (**P2**) just before midnight (22−00 UTC) on that day (solid line). The precipitation associated with P1 is delayed by 4 hours in the COSMOiso simulation compared to the precipitation recorded by the rain gauge network, which shows a peak at 16−18 UTC (grey line with dot in Fig. 2), while the precipitation during P2 phase is closely reproduced by the simulation with a reasonable timing (~1 hour early, with the measured peak occurring at 23−01 UTC). P1 is related to rain from the convection parameterization, and P2 is related to rain associated with large-scale vertical motion. The model, in contrast to the observation, does not produce two peaks in the total precipitation. These peaks can be seen by looking at the two precipitation types separately. In the following, 20 UTC on 15 October and 00 UTC on 16 October are considered as times representative of P1 and P2, respectively, while 16 UTC on 15 October is considered as representative of the pre-HPE conditions.

3.2 Distribution of SWI over the Mediterranean

The moisture structure upstream of the HPE; 1) the presence of an African moisture plume favouring the

efficiency of the convection to produce more precipitation, 2) the importance of southerly flow from the warmer Mediterranean Sea south of Sicily in enhancing the convergence ahead of the cold front, and 3) the role of the upper-level trough over southern France extending to the western Mediterranean in organizing convection at the leading edge of the surface front, highlighted by Lee et al. (2016) has been further studied using SWI data. At 16 UTC on 15 October 2012, an upper-level trough located over south-eastern France~~,~~ extends to northern Algeria. Sea-level pressure values lower than 1002 hPa can be observed over south-eastern France extending to northern Italy (Fig. 3a) with the associated cyclonic flow seen at 850 hPa. Strong northerly mistral and tramontane winds associated with ~~very~~ cold and dry air, with $\delta^{18}O_v$ less than –16‰ and q less than 2 g kg^{-1} (Fig. 4a, b), and thus ~~very~~ low potential temperature, θ, are located over the Gulf of Lion (≤ 300~~2~~ K, dark-blue area in Fig. 3b). Fig. 4a shows two bands of large q values in excess of 6 g kg^{-1} at 850 hPa upstream of the HPE, one over the Tyrrhenian Sea ('TY' box in Fig. 3b) where a cold front is located (large gradient of θ in range of 315–330 K, dashed line in Fig. 3b), and another one across north Africa extending towards SI with south to south-westerly winds where the African moist plume with the values of $\theta \geq 330$ K is located (red area in Fig. 3b), ahead of trough. ~~At the same time, a very warm and moist air mass with high θ values (≥ 330 K, red area in Fig. 3b) is transported from the northern Africa to Sicily at 850 hPa, ahead of the trough, where the south-westerly and southerly winds converge. Over the Tyrrhenian Sea ('TY' box in Fig. 1b), upstream of SI, a large horizontal θ gradient (308−326 K) can be seen at 850 hPa, indicating the elongation of the surface cold front along a southwest to northeast axis.~~At 600 hPa (Fig. 4c), $\delta^{18}O_v$ values in excess of −25 ‰ can be seen at the southern edge of the surface cold front. This signature can be explained by the transport of water vapour to higher levels by updrafts along the front. Another interesting point we can see by comparing the q with the $\delta^{18}O_v$ maps (crescent closed by dashed line, Fig. 4a−b) is that an additional band of enriched water vapour ($\delta^{18}O_v \geq -18$ ‰, Fig. 4b) is found at the southern boundary of the mistral (and the tramontane), in a region of still relatively low q values (≤ 5 g kg^{-1}, Fig. 4a). This SWI-enriched band reflects the moisture brought to higher levels by convective updrafts that develop within the strong mistral outflow over the warm sea surface, typical of cold-air outbreaks. In this region, a band of moderate brightness temperature at 10.8 µm (230−240 K, altitudes about 5−6 km) is measured by the Spinning Enhanced Visible and Infrared Imager on board the geostationary Meteosat Second Generation satellite (not shown, see Fig. 4 of Lee et al., 2016). In the

simulation, weak precipitation is also produced in this region from clouds located mostly below 5 km above sea level (ASL) (not shown).

The hourly evolution of the moist and SWI-enriched air mass over the TY during the period 16−20 UTC can also be seen in the hourly evolution of $\delta^{18}O_v$ in Fig. ~~6~~5, which shows the average $\delta^{18}O_v$ in 1-km deep layers spanning from 1 to 7 km ASL in the TY region from 09 UTC on 15 October to 09 UTC on 16 October together with the average θ values at 850 hPa within TY. From 09 UTC to 19 UTC on 15 October, while the average θ value at 850 hPa is consistently high at 322 K, the $\delta^{18}O_v$ values between 1 and 5 km ASL slightly increase but the $\delta^{18}O_v$ values between 5 and 7 km ASL gradually decrease revealing the arrival of the upper-level trough (Figure ~~6~~5a).

During the two precipitation phases at 20 UTC ~~(Fig. 3c, d)~~ and 00 UTC ~~(Fig. 3e, f)~~, both θ and $\delta^{18}O_v$ drop dramatically (Figs. 5a) with the arrival of the upper-level trough cold front in the TY region (Figs. 3c–f, and 4d–i), ~~the upper-level trough and the cold front propagate towards the south-east~~ while the warm and moist air mass with large q and large $\delta^{18}O_v$ values coming from tropical Africa persists upstream of SI (Fig. 5b). At 20 UTC (Fig. 3c, d), southerly winds (10−15 m~~–~~ s^{-1}) transport the warm and moist air mass with high θ values (≥ 325~~6~~ K) from the Strait of Sicily to SI, and the convection occurred in the high θ region at the southern edge of the front (dashed line in Fig. 3d). The frontal wind convergence of south-westerly and southerly winds (10−15 m s^{-1}) can be seen upstream of the HPE at the 850-hPa level.

Then at 00 UTC when the trough is located in the southern Tyrrhenian Sea with the low-level mistral air mass ($q \leq 3$ g kg^{-1} and $\delta^{18}O_v \leq -24$‰ in Fig. 4g–h) at the ~~north-east~~western edge, strong cyclonic flow can be identified over the SI region while the warm and moist air mass ($\theta \geq$ 325~~8~~ K) over the Strait of Sicily is continuously advected towards SI (Fig. 3~~e~~f). Higher up, at 600 hPa, the trough-related, strongly SWI-depleted air masses descending from higher altitudes show $\delta^{18}O_v$ values lower than −45~~6~~ ‰ (Fig. ~~5~~4i). In contrast to the trough, the African moisture plume is associated with large q values in excess of 10 g kg^{-1} at 850 hPa level extending to the SI region (Fig. 4~~5~~g). As θ decreases from 322 to 300 K in TY (Fig. ~~6~~5a), the $\delta^{18}O_v$ drops more rapidly at altitudes above 3 km compared to the $\delta^{18}O_v$ drop seen in lower altitudes, where the trough-related dry airstreams are moistened by SWI-enriched fresh ocean evaporate. The minimum $\delta^{18}O_v$ value increases lowering the altitudes to near surface, for instance, the minimum $\delta^{18}O_v$ values of −23 and −36 ‰ are seen at

1−2 and 2−3 km ASL respectively, while values lower than −47 ‰ occur at altitudes above 3 km ASL. The hourly evolution of average $\delta^{18}O_v$ in the TY region shows the propagation of the surface front and upper-level trough at altitudes of 1−7 km ASL, and the associated subsidence of dry and cold air. It is worth noting that the arrival timing of cold and dry air subsidence in TY, 19−20 UTC, (Fig. 5~~6~~a) corresponds to the onset of precipitation in SI, 19 UTC (vertical bars, Fig. 2). Overall the synoptic evolution simulated by COSMOiso is similar to the one analysed using an observational dataset by Lee et al. (2016).

4. SWI~~s~~ distribution ~~in the environment of the HPE~~during two precipitation phases

~~*4.1. Distribution of SWIs over the Mediterranean prior to the HPE*~~

~~Figure 5 shows the horizontal distributions of *q* at 850 hPa, and $\delta^{18}O_v$ at 850 and 600 hPa at 16, 20, and at 00 UTC. At 16 UTC, Fig. 5a shows two bands of large *q* values in excess of 6 g kg^{-1} at 850 hPa upstream of the HPE, one over TY where the cold front is located (large horizontal θ gradient in Fig. 3b), and another one across north Africa extending towards SI where the African moist plume is located ($\theta \geq 330$ K, Fig. 3b). The two bands of large *q* are associated with $\delta^{18}O_v$ values larger than −16 ‰ (Fig. 5b), while the mistral and the tramontane, the low-level strong and cold northerly winds, are associated with very low $\delta^{18}O_v$ values, less than −24 ‰. At 600 hPa (Fig. 5c), large $\delta^{18}O_v$ values in excess of −22 ‰ can be seen upstream of the SI area at the southern edge of the surface cold front. This signature can be explained by the transport of water vapour to higher levels by updrafts along the front. Another interesting point we can see by comparing the *q* with the $\delta^{18}O_v$ maps (crescent closed by dashed line, Fig. 5a−b) is that an additional band of enriched water vapour ($\delta^{18}O_v \geq -18$ ‰, Fig. 5b) is found at the southern boundary of the mistral (and the tramontane), over western Corsica and Sardinia, in a region of still relatively low *q* values (≤ 5 g kg^{-1}, Fig. 5a). This SWI-enriched band reflects the moisture brought to higher levels by convective updrafts that develop within the strong mistral outflow over the warm sea surface, typical of cold-air outbreaks. In this region, a band of moderate brightness temperature at 10.8 μm (230−240 K, altitudes about 5−6 km) is measured by the Spinning Enhanced Visible and Infrared Imager on board the geostationary Meteosat Second Generation satellite (not shown, see Fig. 4 of Lee et al., 2016). In the simulation, weak precipitation is also produced in this region from clouds located~~

~~mostly below 5 km above sea level (ASL) (not shown).~~

The temporal evolution of the domain-averaged $\delta^{18}O_v$ in water vapour and q within the SI area at the first model level (approximately 20 m ASL) (Fig. ~~4~~6) shows the different behaviour during IOP 13. While the q value increases gradually to 13.5 g kg^{-1} until 19 UTC, just before P1, the $\delta^{18}O_v$ value maximizes to −13.6 ‰ at 16 UTC and then decreases during P1 to −15 ‰. During P2, the $\delta^{18}O_v$ value increases shortly to −14.6 ‰ whereas the q value continues to decrease to 8 g kg^{-1}. The detailed 3-D history and structure of $\delta^{18}O$ and q of the air parcels associated with P1 and P2 over SI will be shown in the following section.

~~At 20 UTC (Fig. 5d–f), the band with large q and large $\delta^{18}O_v$ values corresponding to the air mass ahead of the cold front moves close to SI, while the African moisture plume has moved further north around the trough. The hourly evolution of the moist and SWI-enriched air mass over the TY during the period 16–20 UTC can also be seen in the hourly evolution of $\delta^{18}O_v$ in Fig. 6, which shows the average $\delta^{18}O_v$ in 1-km deep layers spanning from 1 to 7 km ASL in the TY region from 09 UTC on 15 October to 09 UTC on 16 October together with the average θ values at 850 hPa within TY. From 09 UTC to 19 UTC on 15 October, while the average θ value at 850 hPa is consistently high at 322 K, the $\delta^{18}O_v$ values between 1 and 5 km ASL slightly increase but the $\delta^{18}O_v$ values between 5 and 7 km ASL gradually decrease revealing the arrival of the upper-level trough (Figure 6a).~~

~~From 20 UTC on 15 October to 07 UTC on 16 October 2012, both θ and $\delta^{18}O_v$ values start to drop dramatically with the arrival of the cold front in the TY region (Fig. 6a). At 00 UTC (Fig. 5g) over the Tyrrhenian Sea, where the strong cold and dry cyclonic flow prevails (Fig. 3e and 3f), the mistral is evidenced by very low q values ≤ 2 g kg^{-1} (Fig. 5g) and low $\delta^{18}O_v$ values ≤ −24 ‰ (Fig. 5h) at 850 hPa. Higher up, at 600 hPa, the trough-related, strongly SWI-depleted air masses descending from higher altitudes show $\delta^{18}O_v$ values lower than −46 ‰ (Fig. 5i). In contrast to the trough, the African moisture plume is associated with large q values in excess of 10 g kg^{-1} at 850 hPa level extending to the SI region (Fig. 5g). As θ decreases from 322 to 300 K in TY (Fig. 6a), the $\delta^{18}O_v$ drops more rapidly at altitudes above 3 km compared to the $\delta^{18}O_v$ drop seen in lower altitudes, where the trough-related dry airstreams are moistened by SWI-enriched fresh ocean evaporate. The minimum $\delta^{18}O_v$ value increases lowering the altitudes to near surface, for instance, the minimum $\delta^{18}O_v$ values of −23 and −36 ‰ are seen at 1–2 and 2–3 km ASL respectively, while values lower~~

~~than −47 ‰ occur at altitudes above 3 km ASL. The hourly evolution of average $\delta^{18}O_v$ in the TY region shows the propagation of the surface front and upper-level trough at altitudes of 1−7 km ASL, and the associated subsidence of dry and cold air. It is worth noting that the arrival timing of cold and dry air subsidence in TY, 19−20 UTC, (Fig. 6a) corresponds to the onset of precipitation in SI, 19 UTC (vertical bars, Fig. 2).~~

4.12. ~~SWI distribution during t~~The convective phase of precipitation

4.12.1. History of air parcels and related SWI evolution

This section aims to investigate the history of the air masses involved in the convective precipitation phase P1. Figure 7 displays the history of air parcel arriving at SI in the layer 800−700 hPa at 20 UTC on 15 October 2012. The 3-day backward trajectories shown in Fig. 7 indicate that the air parcels arriving in the SI region in the layer between 800 and 700 hPa at 20 UTC on 15 October are from the North Atlantic. These air parcels are mostly ~~very~~ dry ($q \leq 5$ g kg^{-1}) along the track~~, with q values below 5 g kg^{-1}~~ during the 3 days except for the last 18 hours before their arrival in SI (Fig. 7a). In the period between 48 and 18 hours before their arrival in SI the air parcels descend rapidly from altitudes of 3-5 km to below 1 km ASL over the Tyrrhenian Sea, and below 2.5 km ASL over the Strait of Sicily (Fig. 7d). This penetration of dry air from upper-levels to the surface enhances surface evaporation, leading to a sharp increase of ~~the~~ q as well as ~~the~~ $\delta^{18}O_v$ ~~values~~ (Fig. 7a−c). Between 18 and 6 hours before arrival in SI, the median surface evaporation rate along the trajectories doubles from 0.15 to 0.32 mm h~~r~~$^{-1}$ with a peak 12 hour before the arrival in SI (Fig. 7c). A few air parcels travel over the Strait of Sicily towards SI where mixing with the moist and SWI-enriched moisture plume from North Africa occurs (Fig. 4~~5~~d−f). The median q value~~s~~ along the trajectories increases by a factor of 2.5 from 3.8 to 8.4 g~~−~~ kg^{-1} with the peak 10 hour before arrival in SI, whereas the median $\delta^{18}O_v$ value increases from −27 to −18 ‰ (not shown).

Figure 8 displays the q−$\delta^{18}O_v$ scatter diagram along the entire trajectories seen in Fig. 7 at different times before their arrival at SI. Figure 8 also shows that the q and $\delta^{18}O_v$ values rapidly increase in the last 12 hours prior to arrival in SI. Between 60 and 12 hours before the arrival of the air parcels in SI (Fig. 8a, b), the q and $\delta^{18}O_v$ values are still relatively small, i.e. average q of 2−6 g~~−~~ kg^{-1}, average $\delta^{18}O_v$ between −25 and −19 ‰, in the dry pocket of the upper-level trough. During the last 12 hours (black star, Fig. 8b), ~~the average~~ q is about

9 g– kg^{-1} on average, and the average $\delta^{18}O_v$ is about −17 ‰. During this time, the q–$\delta^{18}O_v$ evolution follows a curve that lies close to a typical Rayleigh line for the Mediterranean condition (SST of 26°C, blue line), indicating the onset of precipitation. Several points fall substantially below this Rayleigh distillation line (solid line, Fig. 8b), suggesting a precipitation recycling by partial re-evaporation of rain drops (Worden et al., 2007).

Between 6 and 3 hours before their arrival in SI, the upper to low-level trajectories (grey to purple dots in Fig. 9a, b) follow a mixing line (orange dashed line) during their descent while the lowermost trajectories (black and grey dots) partly follow a Rayleigh distillation line (blue solid line). This shows that the descending dry air parcels mix with the warm and moist air parcels from lower altitudes, and near-surface which also increases air parcels mix between surface evaporation and background vapour. During P1 (Fig. 9c), the q–$\delta^{18}O_v$ evolution at all levels lies on and below the Rayleigh line, suggesting that air parcels are representative of the convective updraft after condensation of the rain drops (q–$\delta^{18}O_v$ along the Rayleigh curve) and that some air parcels took up the evaporated moisture from falling precipitation.

4.12.2. Horizontal distribution of SWIs

At 20 UTC, the precipitation feature over SI is associated with a region of enhanced convective activity and many multiple convective cells extending from SI to the Strait of Sicily (area closed by dashed line in Fig. 10a) ahead of the surface cold front where westerly and north-westerly winds prevail at 542 m ASL (Fig. 10b) and the frontal south-westerly wind is dominant at 2455 m ASL (Fig. 10cd). Within the precipitation area, relatively low $\delta^{18}O_v$ values (i.e. ≤ −16 ‰) than in the vicinity are found at 542 m ASL while relatively high $\delta^{18}O_v$ values ≥between −19 20 and −2284 ‰ are found at 2455 m and 5565 m ASL, respectively (Fig. 10b=d, f), showing the signature of strong and deep convective mixing that brings SWI-depleted moisture towards the surface within the downdrafts and SWI-enriched moisture is pumped to higher altitudes within the updrafts. This signature is consistent with the temporal evolution of average $\delta^{18}O_v$ in SI. Figure 56b shows a larger $\delta^{18}O_v$ increase at high altitudes of 4−7 km ASL (green to purple lines in Fig. 56b) than at lower altitudes of 1−3 km ASL (black to yellow lines) from 19 to 22 UTC. The SWI-enriched air masses with high $\delta^{18}O_r$ values in rain (≥ −10 ‰), are distributed over the TY region (Fig. 10e=f) and SWI-enriched air masses with high $\delta^{18}O_s$ values in snow (≥ −1620 ‰), are aligned ahead of the cold front over Sicily (Fig 10g). The depletion of water vapour

and the enrichment of rain water and snow over the TY indicate the uptaking by the air mass of evaporated moisture from falling hydrometeors.

At the same time, the African moisture plume is associated with SWI-enriched vapour with large $\delta^{18}O_v$ in excess of −2~~1~~2 ‰ and SWI-enriched snow with ~~larger~~values of $\delta^{18}O_s$ larger~~value~~ than −12 ‰ around~~toward~~ the southern tip of the precipitating area at 5565 m (Fig. 10f~~d~~, g), indicating the continuous supply of the enriched moisture plume from North Africa to SI. We can see this constantly large $\delta^{18}O_v$ values in SI at all altitudes between 1 and 7 km during IOP13 in Fig. 5~~6~~b. The dry pocket of the upper-level trough is distinguished by SWI-depleted vapour air masses with low $\delta^{18}O_v \leq -36$~~7~~ ‰ at 2455 m and 5565 m ASL over Sardinia and Corsica (Fig. 10~~8c, d~~, f).

The Lagrangian analysis indicates that most ~~moist~~of processes inducing precipitation during P1 take place ~~over a very short timescale~~ during the last 18 hours over the Tyrrhenian Sea and the Strait of Sicily. The descending air parcels from the mid troposphere reach altitudes below 1 km ASL at the cold front and take up large amounts of evaporated moisture near the warm sea surface of the Tyrrhenian Sea. Then additional moisture is taken up at altitudes below 2 km ASL from mixing with the African moisture plume that extends from the African continent to the Strait of Sicily. During the period from 18 to 6 hour before the precipitation peak P1, the q and $\delta^{18}O_v$ values strongly increase. At the time of precipitation, strong convective mixing injects~~processes inject the moisture that is~~ SWI-enriched moisture into higher altitudes and depleted moisture to near surface ~~moisture~~ over SI.

4.~~3~~2. ~~SWIs distribution during~~The large-scale phase of precipitation

4.~~3~~2.1. History of air parcel and related SWI evolution

The 3-day backward trajectories in Fig. 11 evidence that the air parcels arriving at SI in the layer between 800 and 700 hPa at 000 UTC on 16 October come from North Africa and partly ~~over~~ from the southern Iberian Plateau. ~~Figure 11a shows that t~~The air parcels are consistently moist along the tracks (Fig. 11a), with average q value~~s~~ mostly ≥ 5 g ~~–~~kg^{-1} along the track, in contrast to the air parcels involved in the P1 phase (see section 4.1~~2~~.1). During the 3 days prior to their arrival in SI, the air parcels are enriched with SWI, showing large $\delta^{18}O_v$ values in excess of −24 ‰, and ~~. T~~the air parcels are located at low altitudes mostly below 2 km ASL

(Fig. 11b, d). They continuously take up water vapour over North Algeria and in the Strait of Sicily (Fig. 11a–b), ~~for instance~~and the median q increases from 6.5 to 9 g~~–~~ kg^{-1} and the median $\delta^{18}O_v$ increases from −18 to −16 ‰ in the period from 72 to 10 hours before the precipitation onset. The air parcels arriving at SI at 00 UTC at higher levels between 700 and 500 hPa are also moist and SWI-enriched, originate from North Africa (not shown), and are related to the moist tropical plume.

These moist and SWI-enriched air parcels are also evident from the scatter diagram of q and $\delta^{18}O_v$. Figure 12 shows the relatively large q and $\delta^{18}O_v$ values during the 3 days prior to their arrival in SI, i.e. q of 5−16 g~~–~~ kg^{-1} (average of 8−10 g~~–~~ kg^{-1}), and $\delta^{18}O_v$ between −12 and –25 ‰ (average in −16 and −18 ‰). During this period, the minimum $\delta^{18}O_v$ of the air parcel gradually increases from −33 to −27 ‰. In particular the moist branch of this q–$\delta^{18}O_v$ distribution lies close to Rayleigh distillation curve (~~blue~~ solid line, Fig. 12a–c) for all 3 days, indicating sustained cloud and precipitation formation. As above, values below this Rayleigh curve point to the importance of precipitation recycling, which also occurs repeatedly during the 3-day period.

4.~~3~~2.2. Horizontal distribution of SWIs

At 00 UTC on 16 Oct. during P2, stronger precipitation than that of P1 is produced, and the precipitation ~~cell~~ system is located mainly over SI (marked area closed by dashed line in Fig. 13a). In the vicinity of the precipitating region, ~~where~~ strong cyclonic south-westerly flow ≥ 25 m~~–~~ s^{-1} is dominant at 2455 m and 5565 m ASL (Fig. 13~~c~~–d, f). Within the precipitating area, water vapour is gradually depleted and $\delta^{18}O_v$ values are relatively low from near the surface (542 m ASL) to mid altitudes of 5565 m ASL (Fig. 13b,~~–~~ d, and f). A strong depletion of isotopes in rain water is seen at 2455 m ASL (Fig. 13e~~f~~). This is due to the steady large-scale ascent of air parcels in front of the trough that lead to cloud formation and rain out. The strong depletion of vapour in lower to mid altitudes is also evident from Fig. 5~~6~~b, which shows decreasing $\delta^{18}O_v$ values from 23 to 01 UTC (black to purple lines). It is worth noting that θ increases continuously until 23 UTC and reaches 327 K in SI (thin line with white circles in Fig. ~~6~~5b), while θ is rather constant before the arrival of the front and trough and the peak value is about 5 K lower in TY compared to SI (thin line with white circles in Fig. ~~6~~5a, b). This reflects the influence of the moisture plume from North Africa. The moist and enriched African moisture plume including high $\delta^{18}O_v$ of vapour in excess of −2~~6~~ ‰ is advected by the strong south-westerly

flow from the Strait of Sicily to SI (Fig. 13~~c~~–d). This is consistent with the rapid re-enrichment of vapour in SI after the precipitation (Fig. 5~~6~~b). Then after 04 UTC, with the arrival of the front and upper-level trough, the vapour becomes more depleted at all levels (Fig. 5~~6~~b).

The Lagrangian analysis indicates that the moistures that feeds the convection during P2 is coming from ~~air parcels that bring moisture from~~ North Africa and the air parcels take up additional moisture (2−3 g– kg^{-1}) over the Mediterranean. These air parcels carry moist and SWI-enriched air at layers below 2 km ASL. With the arrival of the upper-level trough over the southern Tyrrhenian Sea, strong cyclonic flow leads to the ~~entrainment~~ mixing of air from the African moist plume to SI. During P2, the gradual depletion of water vapour takes a place at SI at all levels.

5. Conclusion

~~During IOP 13 (~~On 15 to 16 October 2012~~) of the HyMeX SOP 1~~, SI experiences a HPE (total precipitation of 62.4 mm) with two phases of precipitation. The first one (P1) is induced by moist convection~~ve~~, while the second one (P2) is mainly associated with large-scale uplift along a front. The moisture transport and processes responsible for the HPEs that occurred over the SI area during IOP 13 have been analysed here using SWI data obtained from a numerical simulation with COSMO$_{iso}$ at 7-km horizontal resolution. The main findings are summarized in two schematic illustrations (Fig. 14).

The 3-day backward trajectory analysis shows that the air parcels arriving in SI during P1 originate from the North Atlantic and descend within the upper-level trough over the north-western Mediterranean Sea. The SWI-depleted air mass (median $\delta^{18}O \leq -45$ ‰) within the descending air parcels ~~arriving at very low levels (below 1 km) are very dry and SWI-depleted (median $\delta^{18}O \leq -25$ ‰, water vapour mixing ratio, $q \leq 2$ g kg^{-1}),~~ ~~and~~ rapidly take up a large amount of water vapour from ocean evaporation (green~~grey~~ encapsulated area in Fig. 14a) ~~. As a consequence, it becomes enriched in SWI ($\delta^{18}O_v \geq -14$ ‰) in a very short time span~~ over the Tyrrhenian Sea and also ~~probably by taking up~~from evaporated moisture from falling precipitation ~~as hinted by the analysis of the trajectory data in the q–δ space (points falling below the Rayleigh distillation line)~~. Additional moisture is taken up over the Strait of Sicily ~~at altitudes below 2 km ASL~~ from mixing with the enriched moisture plume coming from Africa ($\delta^{18}O_v \geq -16$~~2~~ ‰). The SWI-enriched low-level air masses

arriving upstream of SI are convectively pumped to higher altitudes, producing precipitation over SI, and the SWI-depleted moisture is transported towards the surface within the downdrafts ahead of the cold front (red and blue arrows, Fig. 14a).

During P2 (Fig. 14b), just a few hours after P1, the origin of the air parcels arriving at SI is ~~totally different~~distinct, i.e. mostly from North Africa. The air parcels are moist and associated with large $\delta^{18}O$ values (bottom most arrow, median $\delta^{18}O_v \geq -162$ ‰~~, median $q \geq 6$ g kg^{-1}~~). With the arrival of the upper-level trough ($\delta^{18}O_v \leq -458$ ‰ ~~at 600 hPa~~) and ~~low-level~~ mistral ($\delta^{18}O_v \leq -254$ ‰ ~~at 850 hPa~~) over the southern Tyrrhenian Sea, the strong cyclonic flow around the trough (grey dashed line in Fig. 14b) induces the advection of the moist plume towards SI and leads to large-scale uplift of the warm and moist African air mass along the cold front. It brings moisture and leads to gradual rain out of the air parcels over Italy ~~(following Rayleigh distillation)~~. For the convective precipitation phase (P1), most of the moisture processes producing the HPE take place during the last 18 hours before the arrival over SI, while the large-scale advection of SWI-enriched moisture from the African plume by strong cyclonic flow lasts about 72 hours during the large-scale precipitation phase (P2). In both phases, the air parcels take up substantial amount of water vapour over the Mediterranean.

Using the hourly 3-D water vapour isotope data, we highlight the large variety of moisture sources and transport pathways that induced the two phases of the HPE in South Italy during IOP13, and the isotopic characteristics of various air masses associated with the upper-level trough, cold front, mistral, and African moist plume, that were involved in convection development. We also highlight the role of the upper-level trough over the south Tyrrhenian Sea in driving the advection of the SWI-enriched plume from North Africa into the region of the deep convective system resulting in heavy precipitation over SI. Moreover, we demonstrate the importance of various moist processes such as mixing, condensation, and re-evaporation along the pathway based on the q–δ analysis using 3D SWI fields. Although our study is entirely based on a model simulation, the results suggest that the information on mesoscale moist dynamical processes and moisture transport that is contained in SWI, when combined with SWI observations, can provide very useful constrains on the representation of such processes in numerical models.

Our study is the first study to investigate the potential benefit of SWI in the context of a HPE in the

Mediterranean. As such, our study provides a proof of concept of the usefulness of SWI data to understand the variety of origins and moist processes associated with air masses feeding the convection over SI. This will be further investigated in future research using SWI measurements obtained from various platforms, e.g. ground-based, near surface, airborne (Sodemann et al., 2017), and space-borne. Our modelling study will also allow designing forthcoming tailored field campaigns in the Mediterranean region. In this study, COSMOiso simulation at a horizontal grid spacing of about 7 km with parameterized convection results from a trade-off between having high enough resolution for including detailed dynamics of the mesoscale systems and being able to run efficiently over a large domain (about 4,300 km × 3,500 km) that includes the moisture plume over North Africa. This setup allows addressing the question we are interested in, namely: which isotope signals are due to local processes, and which are due to large-scale advection? ~~In addition, t~~To further study the details of the fractionation processes in and around deep convective systems, complementary investigations will be conducted using higher resolution convection-permitting simulation with a 2 km grid to shed a light on cloud microphysical processes inside deep convection.

Author contribution

KOL, FA, SP and CF planned the manuscript and analyses. SP and KOL designed the numerical simulation and SP performed it. JLL and JPC contributed to discussion. KOL prepared the manuscript with contributions from all co-authors.

Acknowledgements

This work was supported by the French Agence Nationale de la Recherche (ANR) via the IODA-MED Grant ANR-11-BS56-0005, the MUSIC grant ANR-14-CE01-014 and the MISTRALS/HyMeX programme.

References

Aemisegger, F. and Papritz, L.: A climatology of strong large-scale ocean evaporation event. Part I: Identification,

global distribution, and associated climate conditions. J. Climate, 31, 7287–7312, doi:10.1175/JCLI-D-17-0591.1, 2018.

Aemisegger, F., Spiegel, J. K., Pfahl, S., Sodemann, H., Eugster, W., and Wernli, H.: Isotope meteorology of cold front passages: A case study combining observations and modelling. Geophys. Res. Lett., 42, 5652−5660, doi:10.1002/2015GL063988, 2015.

Aemisegger, F. and Sjolte, J.: A climatology of strong large-scale ocean evaporation event. Part II: Relevance for the deuterium excess signature of the evaporation flux. J. Climate, 31, 7313–7336, doi:10.1175/JCLI-D-17-0592.1, 2018.

Barthlott C, Davolio S. 2015. Mechanisms initiating heavy precipitation over Italy during the HyMeX Special Observation Period 1: A numerical case study using two mesoscale models. *Q. J. R. Meteorol. Soc.* DOI: 10.1002/qj.2630.

Blossey, P. N., Huang, Z., and Romps, D. M.: Isotopic composition of water in the tropical tropopause layer in cloud-resolving simulations of an idealized tropical circulation, J. Geophys. Res., 115, D24309, doi: 10.1029/2010JD014554, 2010.

Bonne, J. L., Masson-Delmotte, V., Cattani, O., Delmotte, M., Risi, C., Sodemann, H., and Steen-Larsen, H. C.: The isotopic composition of water vapor and precipitation in Ivittuut, southern Greenland, Atmos. Chem. Phys., 14(9), 4419–4439, 2014.

Christner, E., Aemisegger, F., Pfahl, S., Werner, M., Cauquoin, A., Schneider, M., Hase, F., Barthlott, S., and Schädler, G.: The climatological impacts of continental surface evaporation, rainout, and subcloud processes on δD of water vapor and precipitation in Europe. Journal of Geophysical Research: Atmospheres, 123, 4390–4409. https://doi.org/10.1002/2017JD027260, 2018.

Davies, H. C.: A lateral boundary formulation for multi-level prediction models, Q. J. Roy. Meteor. Soc., 102, 405−418, 1976.

Dessler, A., and Sherwood, S.: A model of HDO in the tropical tropopause layer, Atmos, Chem, Phys., 3, 4489–4501, 2003.

Doms, G., Förstner, J., Heise, E., Herzog, H. J., Raschendorfer, M., Schrodin, R., Reinhardt, T., and Vogel, G.: A description of the nonhydrostatic regional model LM. Part II: Physical parameterization, Deutscher

Wetterdienst, Offenbach, Germany, 2005.

Ducrocq, V., Braud, I., Davolio, S., Ferretti, R., Flamant, C., Jansa, A., Kalthoff, N., Richard, E., Taupier-Letage, I., Ayral, P.A., Belamari, S., Berne, A., Borga, M., Boudevillain, B., Bock, O., Boichard, J. L., Bouin, M. N., Bousquet, O., Bouvier, C., Chiggiato, J., Ciimini, D., Corsmeier, U., Coppola, L., Cocquerez, P., Defer, E., Delanoë, J., Di Girolamo, P., Doerenbecher, A., Drobinski, P., Dufournet, Y., Fourrié, N., Gourley, J.J., Labatut, L., Lambert, D., Le Coz, J., Marzano, F.S., Molinié, G., Montani, A., Nord, G., Nuret, M., Ramage, K., Rison, W., Roussot, O., Said, F., Schwarzenboeck, A., Testor, P., Van Baelen, J., Vincendon, B., Aran, M., and Tamayo, J.: HyMeX-SOP1: The Field Campaign Dedicated to Heavy Precipitation and Flash Flooding in the Northwestern Mediterranean. Bull. Am. Meteorol. Soc. 95, 1083−1100, doi:10.1175/BAMS-D-12-00244.1, 2014.

Duffourg, F. and Ducrocq, V.: Assessment of the water supply to Mediterranean heavy precipitation: A method based on finely designed water budgets. Atmos. Sci. Lett. 14, 133−138, 2013.

Duffourg, F., Lee, K. O., Ducrocq, V., Flamant, C., Chazette, P., and Girolamo, P. D.: Role of moisture patterns in the backbuilding formation of HyMeX IOP13 heavy precipitation system, Q. J. Roy. Meteor. Soc., 144: 291−303, doi:10.1002/qj.3201, 2018.

Dütsch, M., Pfahl, S., Meyer, M., and Wernli, H.: Lagrangian process attribution of isotopic variations in near-surface water vapour in a 30-year regional climate simulation over Europe. Atmos. Chem. Phys., 18, 1653–1669, https://doi.org/10.5194/acp-2017-744, 2018

Galewsky, J., and Hurley, J. V.: An advection-condensation model for subtropical water vapor isotopic ratios. J. Geophys. Res., 115, D16116, doi:10.1029/2009JD013651, 2008.

Galewsky, J., Steen-Larsen, H. C., Field, R. D., Worden, J., Risi, C., and Schneider, M.: Stable isotopes in atmospheric water vapor and applications to the hydrologic cycle. Rev. Geophys., 54, doi: 10.1002/2015RG000512, 2012.

Jacob, J. and Sonntag, C.: An 8-year record of the seasonal variation of ^{2}H and ^{18}O in atmospheric water vapour and precipitation at Heidelberg, Germany, Tellus B, 43, 291−300, doi:10.1034/j.1600-0889.1991.t01-2-00003.x, 1991.

Jaussaume, J., Sadourny, R., and Jouzel, J.: A general circulation model of water isotope cycles in the atmosphere,

Nature, 311, 24−29, 1984.

Jouzel, J., Masson-Delmotte, V., Stiévenard, M., Landais, A., **Vimeux, F.**, and Johnsen S. J.: Sveinbjornsdottir and White J.W.C., Rapid deuterium excess changes in Greenland ice cores: a link between the ocean and the atmosphere, *CRAS*, 337, 957-969, **2005**.

Lacour, J. L., Flamant, C., Risi, C., Clerbaux, C., and Coheur, P. F.: Importance of the Saharan heat low in controlling the north Atlantic free tropospheric humidity budget deduced from IASI δD observation. Atmos. Chem. Phys., 17, 9645−9663, 2017.

Lee, K. O., Flamant, C., Ducrocq, V., Duffourg, F., Fourrié, N., and Davolio, S.: Convective initiation and maintenance processes of two back-building mesoscale convective systems leading to heavy precipitation events in Southern Italy during HyMeX IOP 13. Q. J. R. Meteorol. Soc, 142, 2623−2635, doi: 10.1002/qj.2978, 2016.

Lee, K. O., Flamant, C., Ducrocq, V., Duffourg, F., Fourrié, N., Delanoë, J., and Bech, J.: Initiation and development of a mesoscale convective system in the Ebro River Valley and related heavy precipitation over northeastern Spain during HyMeX IOP15a. Q. J. R. Meteorol. Soc, 143, 942−956, doi: 10.1002/qj.2851, 2017.

Lee, K. O., Flamant, C., Duffourg, F., Ducrocq, V., and Chaboureau, J.-P.: Impact of upstream moisture structure on a back-building convective precipitation system in south-eastern France during HyMeX IOP 13. Atmos. Chem. Phys., Discuss, http://doi.org/10.5194/acp-2018-707, 2018.

Lin, Y. L., Chiao, S., Wang, T. A., Kaplan, M. L., and Weglarz, R. P.: Some common ingredients for heavy orographic rainfall. *Wea. Forecasting*, 16, 633−660, 2001.

Martius, O., Zenklusen, E., Schwierz, C., and Davies, H. C.: Episodes of Alpine heavy precipitation with an overlying elongated stratospheric intrusion: A climatology. Int. J. Climatol. 26, 1149−1164, doi: 10.10002/joc.1295, 2006.

Noon, D.: The influence of midlatitude and tropical overturning circulation on the isotopic composition of atmospheric water vapor and Antarctic precipitation. J. Geophys. Res., 113, D04102, doi:10.1029/2007JD008892, 2008.

Noon, D.: Pairing measurement of the water vapor isotope ratio with humidity to deduce atmospheric moistening and dehydration in the tropical midtroposphere. J. Climate, 25, 4476−4494, doi: 10.1175/JCLI-D-11-00582.1, 2012.

Nuissier, O., Ducrocq, V., Ricard, D., Lebeaupin, C., and Anquetin, S.: A numerical study of three catastrophic precipitating events over southern France. I: Numerical framework and synoptic ingredients. Q. J. R. Meteorol. Soc. 134, 111−130, 2008

Nuissier, O., Joly, B., Joly, A., Ducrocq, V., and Arbogast, P.: A statistical downscaling to identify the large-scale circulation patterns associated with heavy precipitation events over southern France. Q. J. R. Meteorol. Soc. 137, 1812−1827. doi:10.1002/qj.866, 2011.

Pfahl, S. and Wernli, H.: Air parcel trajectory analysis of stable isotopes in water vapor in the eastern Mediterr anean, J. Geophys. Res., 113, D20104, doi: 10.1029/2008JD009839, 2008.

Pfahl, S., Wernli, H., and Yoshimura, K.: The isotopic composition of precipitation from a winter storm – a case study with the limited-area model COSMOiso. Atmos. Chem. Phys., 12, 1629−1648, doi: 10.5194/acp-12-1629-2012, 2012.

Ricard, D., Ducrocq, V., and Auger, L.: A climatology of the mesoscale environment associated with heavily precipitating events over a northwestern mediterranean area. J. Appl. Meteorol. Climatol. 51, 468−488. doi:10.1175/JAMC-D-11-017.1, 2012.

Risi, C., Bony, S., and Vimeux, F.: Influence of convective processes on the isotopic composition (O18 and D) of precipitation and water vapour in the Tropics: Part 2: Physical interpretation of the amount effect. J. Geophys. Res. 113, 2008.

Risi, C., Bony, S., Vimeux, F., Chong, M., and Descroix, L.: Evolution of the water stable isotopic composition of the rain sampled along Sahelian squall lines, Q. J. R. Meteorol. Soc., 136: 227−242, doi:10.1002/qj.485, 2010.

Röhner, L., Nerding, K.-U., and Corsmeier, U.: Diagnostic study of a HyMeX heavy precipitation event over Spain by investigation of moisture trajectories. Q. J. R. Meteorol. Soc., 142 (Suppl 1): 287−297, doi:10.1002/qj.2825

Schneider, M., Wiegele, A., Barthlott, S., González, Christner, E., Dyroff, C., García, O. E., Hase, F., Blumenstock, T., Sepúlveda, E., Tsidu, G. M., Kenea, S. T., Rodríguez, and Andrey, J.: Accomplishments of the MUSICA project to provide accurate, long-term, global and high-resolution observations of tropospheric {H2O, δD} pairs – a review, Atmos. Meas. Tech., 9, 2845−2875, 2016.

Sherwood, S., and Dessler, A.: On the control of stratospheric humidity, Geophys, Res, Lett, 27(16), 2513–2516, 2000.

Sodemann, H., Aemisegger, F., Pfahl, S., Bitter, M., Corsmeier, U., Feuerle, T., Graf, P., Hankers, R., Jsiao, G., Schulz, H., Wieser, A., and Wernli, H.: The stable isotopic composition of water vapour above Corsica during the HyMeX SOP1 campaign: insight into vertical mixing processes from lower-tropospheric survey flights. Atmos. Chem. Phys., 17, 6125−6151, 2017.

Sprenger, M. and Wernli, H.: The LAGRANTO Lagrangian analysis tool – version 2.0, Geosci. Model Dev., 8, 2569-2586, 2015.

Steppeler, J., Doms, G., Schättler, U., Bitzer, H. W., Gassmann, A., Damrath, U., and Gregoric, G.: Meso-gamma scale forecast using the nonhydrostatic model LM, Meteorol. Atmos. Phys., 82, 75−96, 2003.

Sturm, K., Hoffmann, G., Langmann, B., and Stichler, W.: Simulation of delta O-18 in precipitation by the regional circulation model REMOiso, Hydrol. Process, 19, 3425−3444, doi:10.1002/hyp.5979, 2005.

Tiedtke, M.: A comprehensive mass flux scheme for cumulus parameterization in large-scale models, Mon. Weather Rev., 117, 1779−1800, 1989.

Tremoy, G., Vimeux, F., Soumana, S., Souley, I., Risi, C., Favreau, G., and Oi, M.: Clustering mesoscale convective systems with laser-based water vapor delta O-18 monitoring in Niamey (Niger), J. Geophys. Res., 119, 5079−5103, doi:10.1002/2013jd020968, 2014.

Turato, B., Reale, O., and Siccardi, F.: Water vapour sources of the October 2000 Piedmont flood. *J. Hydrometeorol.* 5, 693−712, doi:10.1175/1525-7541(2004)005<0693:WVSOTO>2.0CO;2, 2004.

Vimeux, F., Masson, V., Jouzel, J., Petit, J., Steig, E., Stievenard, M., Vaikmae, R. and White, J. W. C.: Holocene hydrological cycle changes in southern hemisphere documented in Antarctic deuterium excess records, *Climate Dynamics,* 17/7, 503−513, **2001.**

Wernli, H. and Davies, H. C.: A Lagrangian-based analysis of ex- tratropical cyclones. I: The method and some applications, Q. J. R. Meteorol. Soc, 123, 467–489, 1997.

Winschall, A., Pfahl, S., Sodemann, H., and Wernli, H.: Impact of north Atlantic evaporation hot spots on southern Alpine heavy precipitation events. Q. J. R. Meteorol. Soc. 138, 1245−1258, doi: 10.1002/qj.987, 2012.

Winschall, A., Sodemann, H., Pfahl, S., and Wernli, H.: How important is intensified evaporation for Mediterranean precipitation extremes? J. Geophys. Res. Atmos. 119, 5240–5256, 2014.

Worden, J., Noone, D., Bowman, K., and Beer, R.: Importance of rain evaporation and continental convection in the

tropical water cycle, Nature, 445, 528–532, 2007.

Yoshimura, K., Kanamitsu, M., Noone, D., and Oki, T.: Historical isotope simulation using Reanalysis atmospheric data, J. Geophys. Res., 113, D19108, doi:10.1029/2008JD010074, 2008.

Yoshimura, K., Kanamitsu, M., and Dettinger, M.: Regional downscaling for stable water isotopes: A case study of an atmospheric river event, J. Geophys. Res., 115, D18114, doi:10.1029/2010JD014032, 2010.

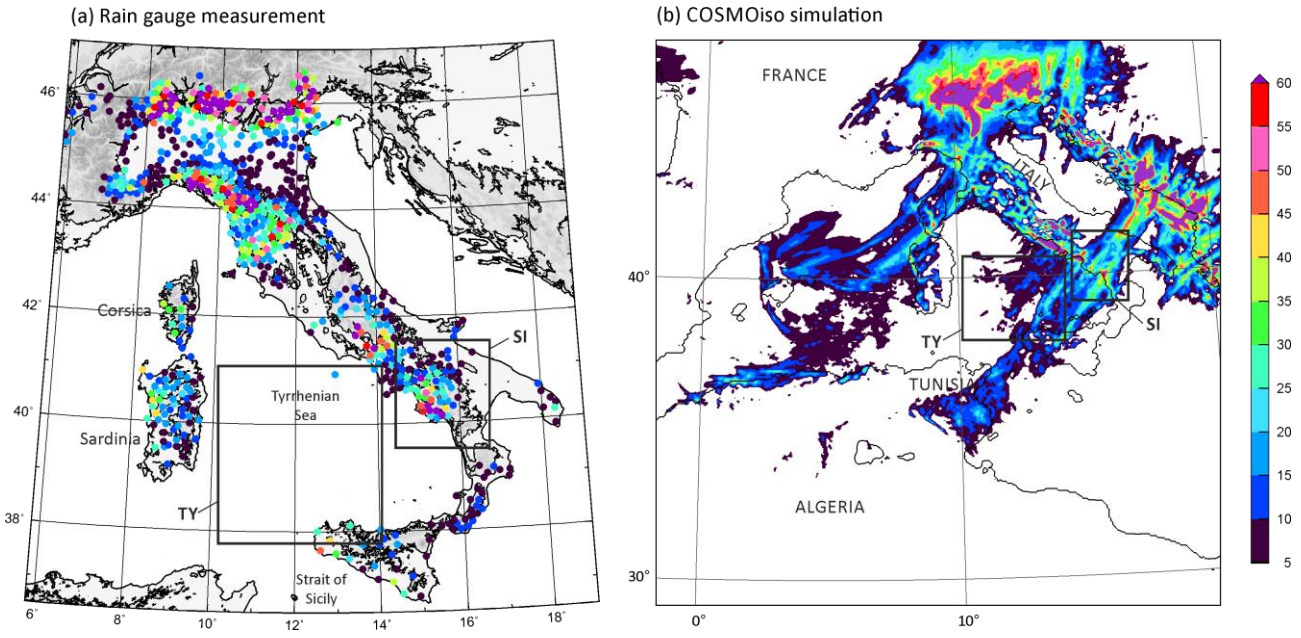

Figure 1. Accumulated precipitation during IOP 13 from 00 UTC on 15 October 2012 to 03 UTC on 16 October 2012 obtained from (a) rain gauge network, and (b) COSMOiso simulation.

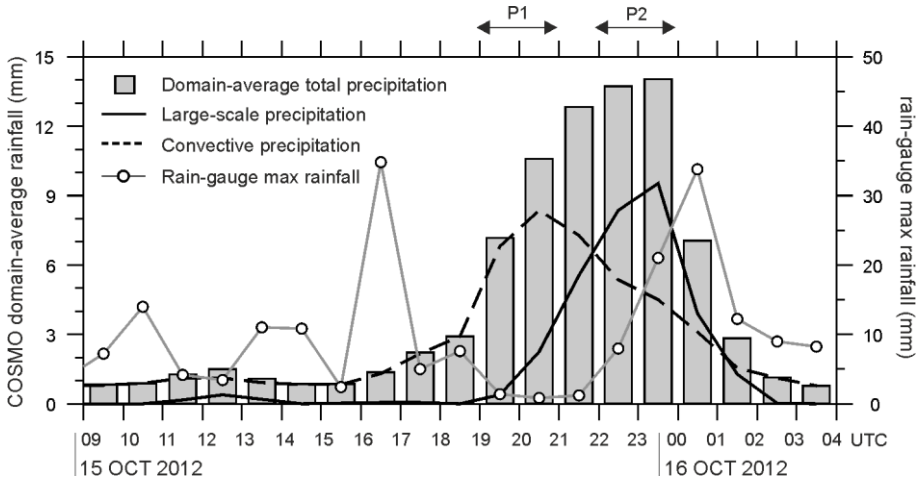

Figure 2. COSMOiso-produced domain-averaged total precipitation (bar), synoptic precipitation (black solid line), and convective precipitation (dashed line) in domain of South Italy (**SI**) over the land during IOP 13. Temporal evolution of observed maximum rainfall within the SI domain is shown by a line with dot. The location of domain SI is depicted by the box in Figure 1.

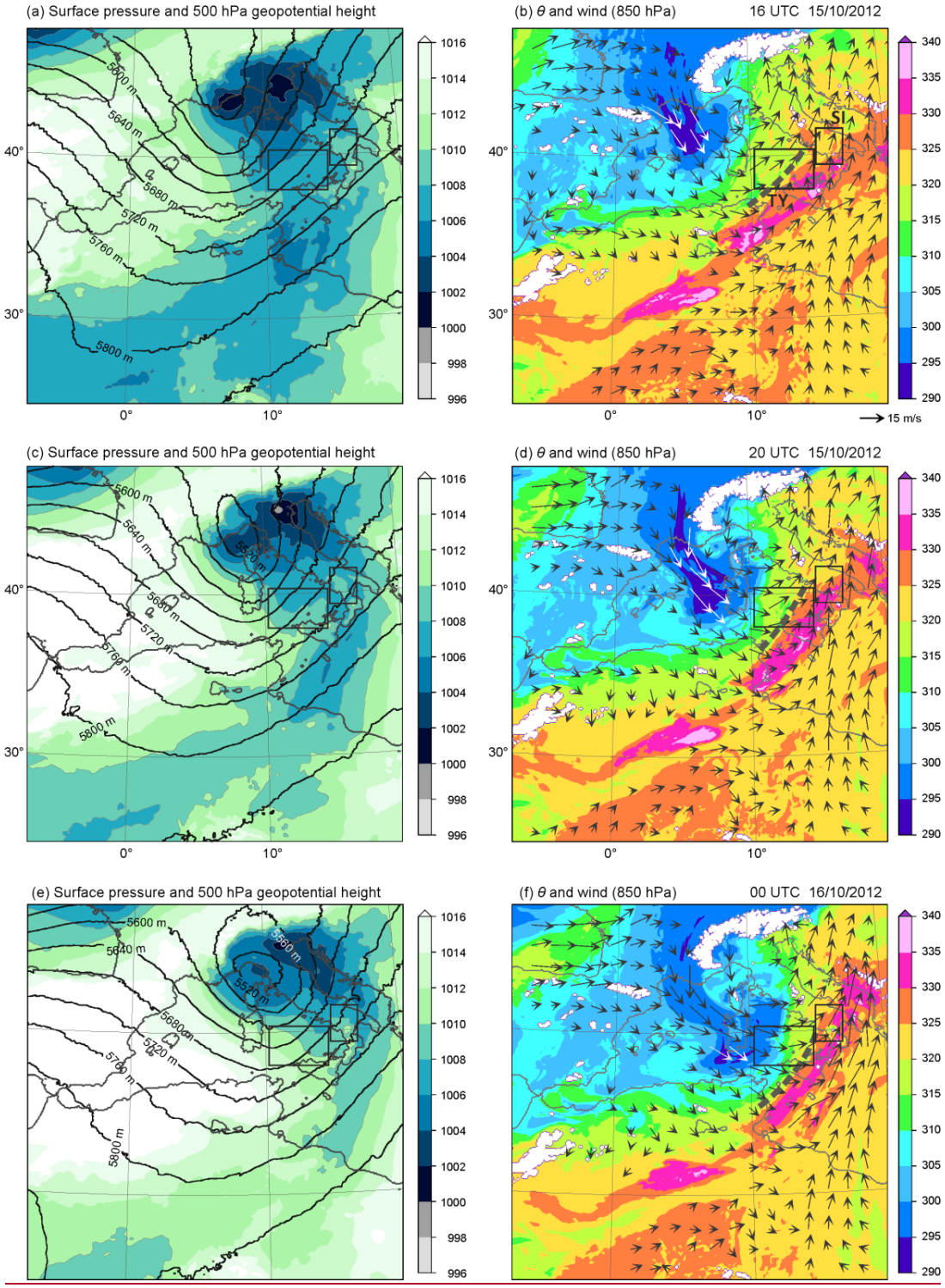

Figure 3. Horizontal distributions of sea level pressure (shades) and ~~horizontal wind~~geopotential height ~~(black arrows)~~ at ~~8~~500 hPa (contour) (left), and potential temperature, θ (shades), and wind (black and white arrows) at 850 hPa (right) at 16 UTC (top) and at 20 UTC (middle) 15 October 2012, and 00 UTC on 16 October 2012 (bottom) produced by the COSMOiso simulation. Coastal line is depicted by black line. The location of cold front is depicted by a dashed line in right panels.

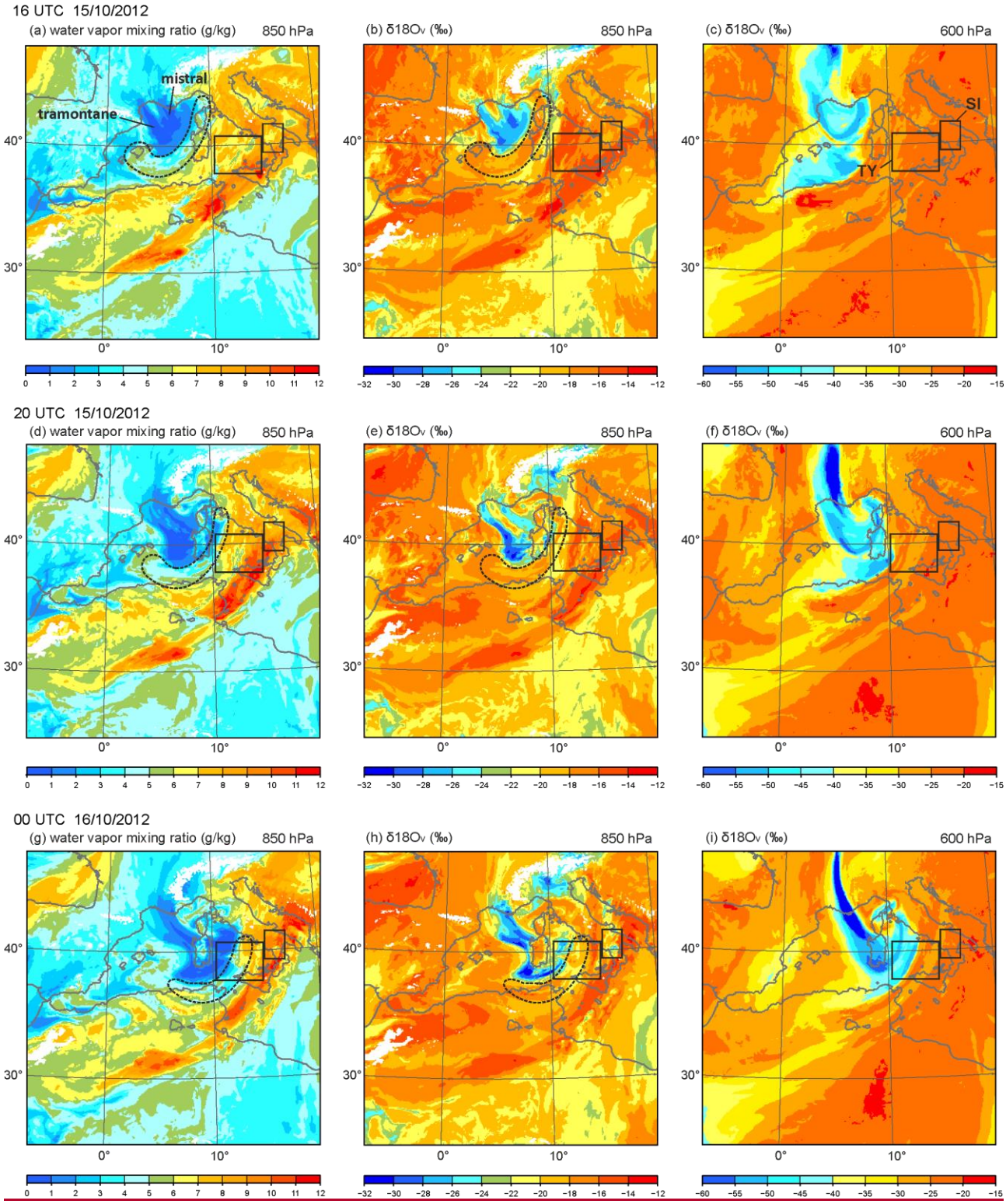

Figure ~~54~~. Horizontal distributions of water vapour mixing ratio at 850 hPa (left), $\delta^{18}O_v$ at 850 hPa (middle) and $\delta^{18}O_v$ at 600 hPa (right) at 16 UTC (top) and 20 UTC (middle) on 15 October 2012, and 00 UTC on 16 October 2012 (bottom).

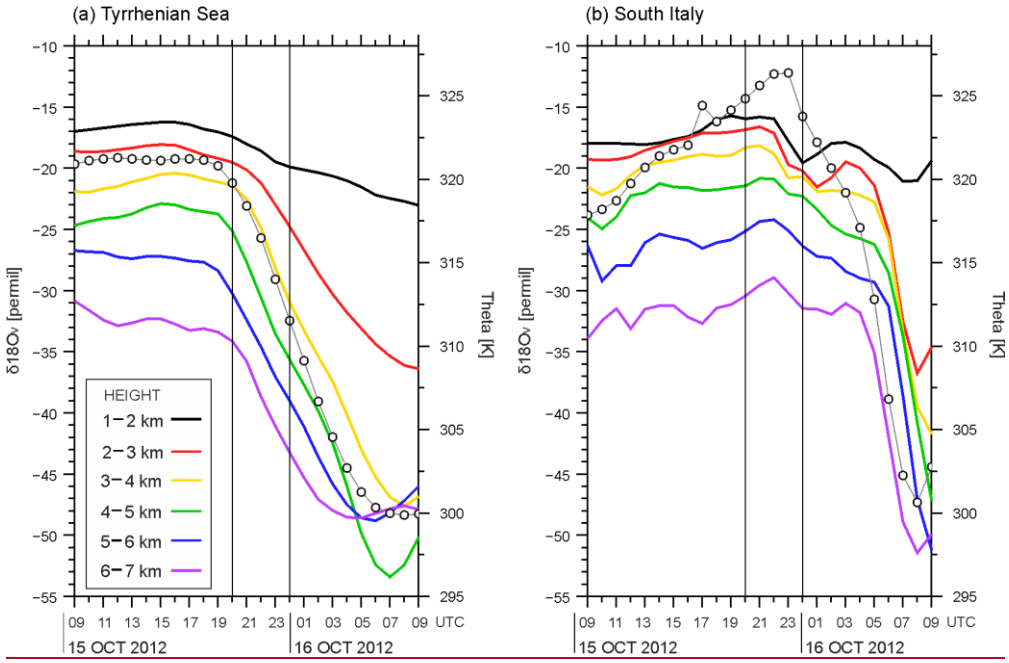

Figure ~~6~~5. The averaged values of potential temperature (θ, K) at 850 hPa (thin line with dot) and $\delta^{18}O_v$ (‰) at altitudes of 1−2 km ASL (black), 2−3 km ASL (red), 3−4 km ASL (yellow), 4−5 km ASL (green), 5−6 km ASL (blue), 6−7 km ASL (purple) over the sea surface upstream the HPE of IOP 13 within domains of (a) Tyrrhenian Sea (marked by 'TY' in Figures 1, 3 and ~~5~~4) and (b) South Italy (marked by 'SI') from 09 UTC on 15 October 2012 to 09 UTC on 16 October 2012.

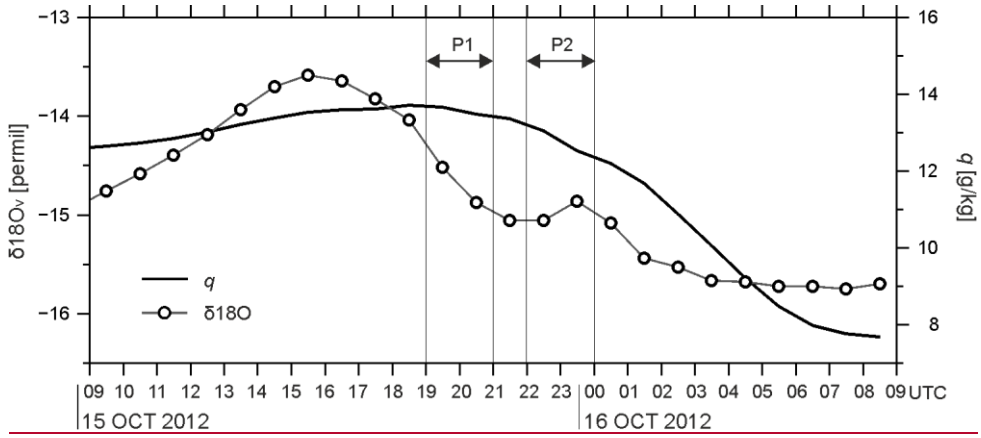

Figure ~~4~~6. Domain-averaged $\delta^{18}O_v$ (line with dot) and q (thick line) in domain of South Italy (**SI**) at the first model level (approximately 20 m height) (limited to the grid point where the topography is lower than 20 m), from 09 UTC on 15 October 2012 to 09 UTC on 16 October 2012. The location of domain SI is depicted by the box in Figures 1 ~~and~~ 3, and 4.

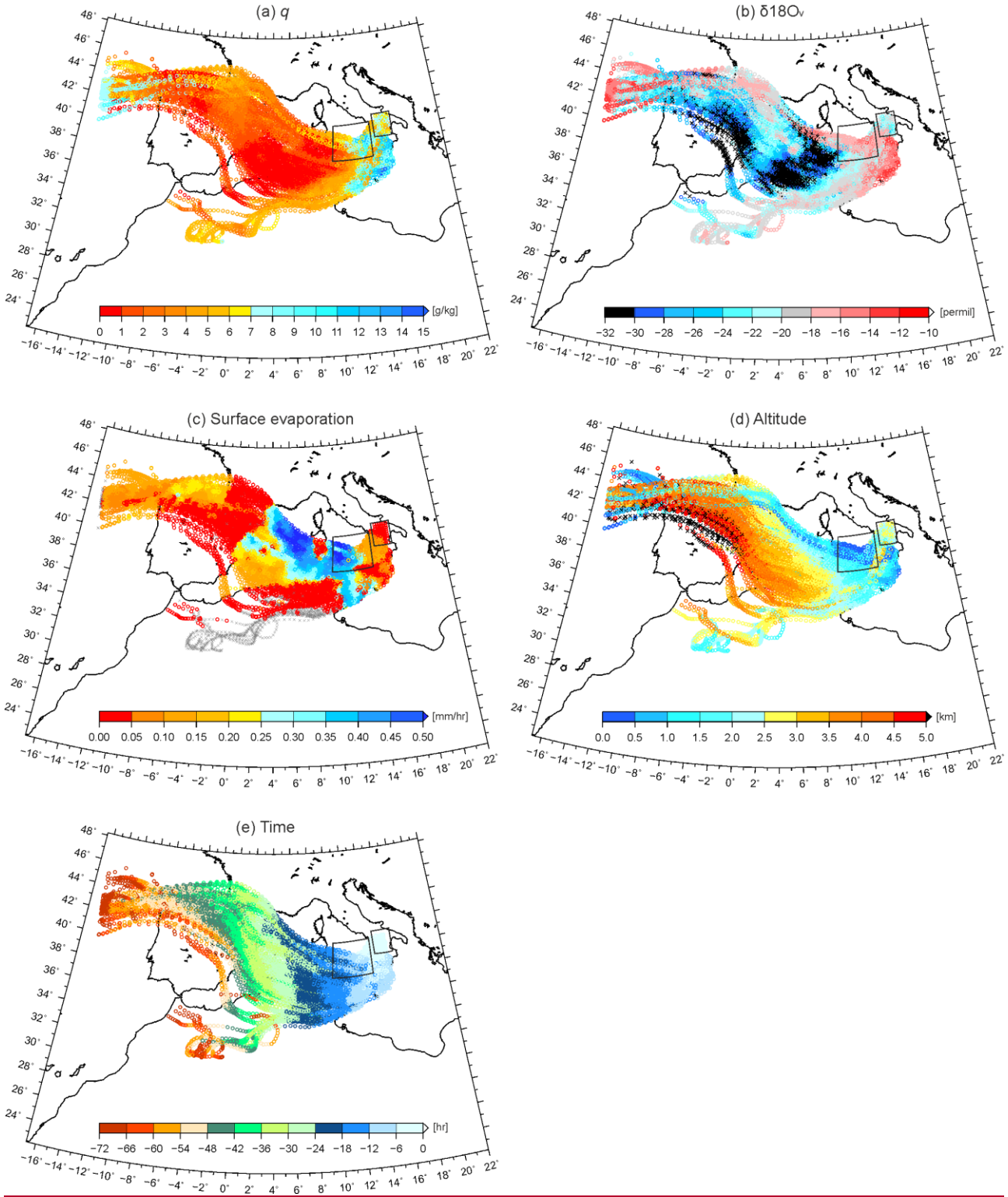

Figure 7. History of air parcel arriving at **SI** in layer of 800−700 hPa at 20 UTC on 15 October 2012. (a) water vapour mixing ratio, q (g kg^{-1}), (b) $\delta^{18}O_v$ (‰), (c) surface evaporation (mm h~~r~~$^{-1}$), (d) altitude (km), and (e) time (h~~r~~).

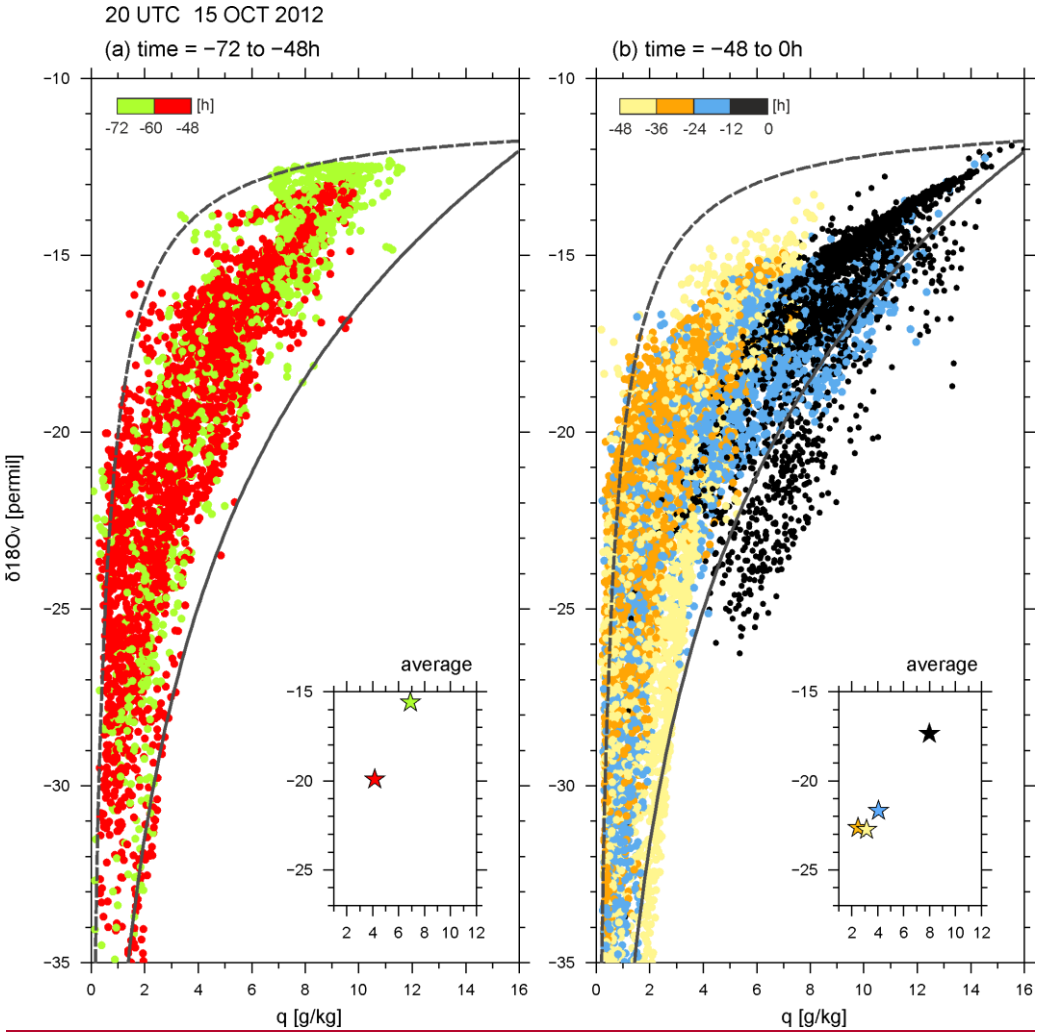

Figure 8. Scatter diagram of q and $\delta^{18}O_v$ along the backward trajectories of Figure 7 during (a) the times between −72 and −48 h~~r~~, and (b) times between −48 and 0 h~~r~~ every 12 hours from 20 UTC on 15 October 2012. The colour of dot changes every 12 h. The mixing and Rayleigh lines are indicated in each panel by ~~orange~~ dashed ~~line~~ and ~~blue~~ solid line, respectively. The averaged q and $\delta^{18}O_v$ every 12 hours is displayed in the bottom right corner of each panel.

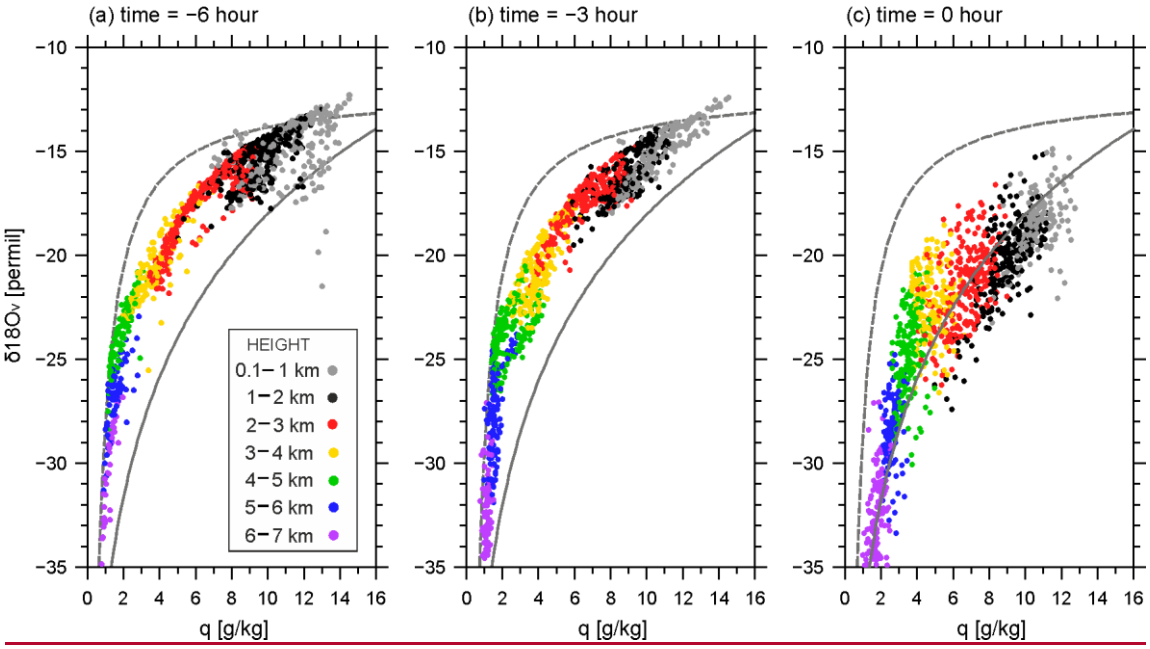

Figure 9. Scatter diagram of q and $\delta^{18}O_v$ along the backward trajectories of Figure 7 but for all altitudes of 1−2 km (black dots), 2−3 km (red dots), 3−4 km (yellow dots), 4−5 km (green dots), 5−6 km (blue dots), and 6−7 km (purple dots) at (a) −6 h~~r~~, (b) −3 h~~r~~, and (c) 0 h~~r~~ from 20 UTC on 15 October 2012. The mixing and Rayleigh lines are indicated in each panel by ~~orange~~ dashed ~~line~~ and ~~blue~~ solid line, respectively.

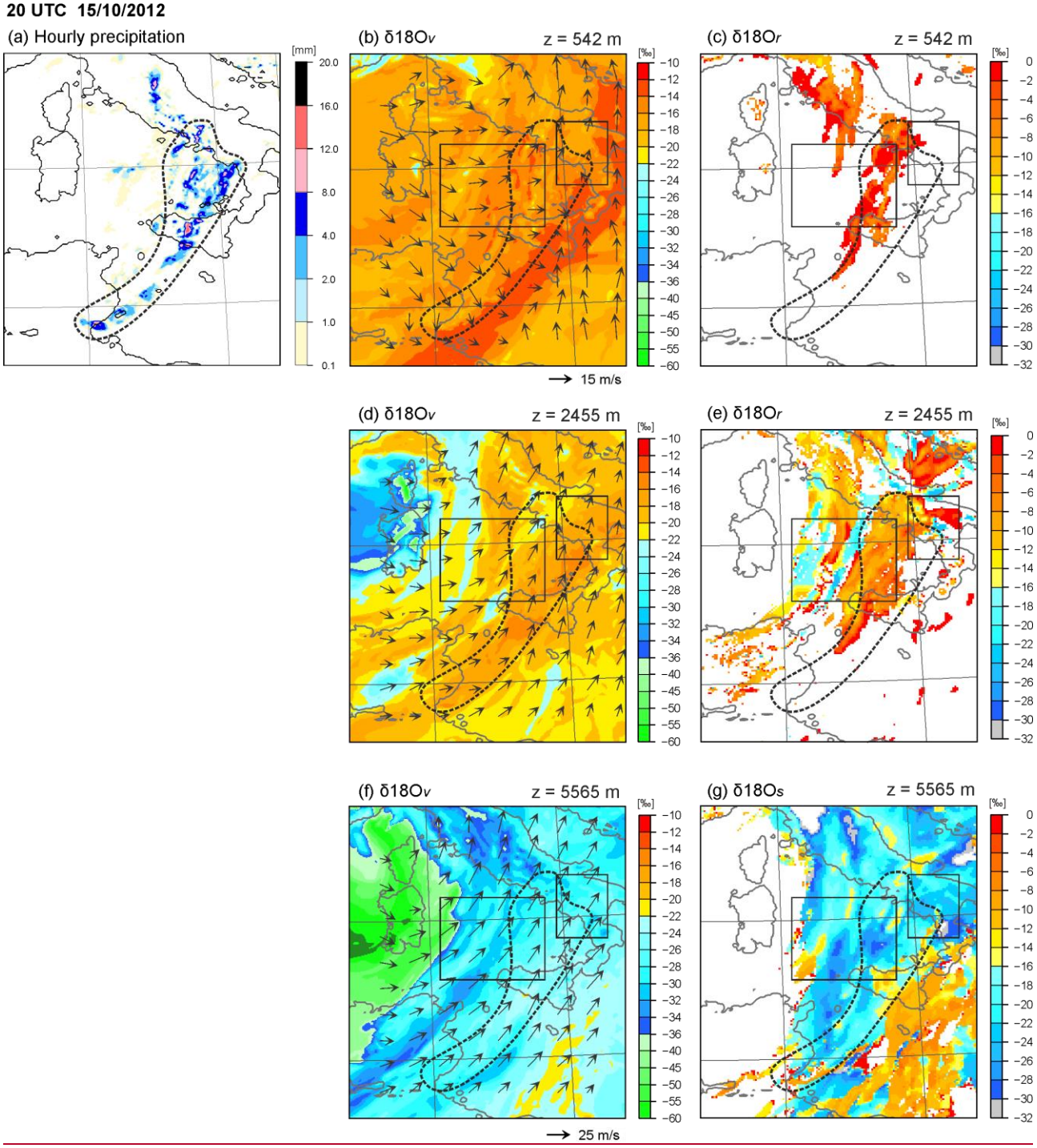

Figure 10. Horizontal distributions of (a) surface hourly precipitation (mm), $\delta^{18}O_v$ (‰) at (b) model level 8 (about 542 m ASL), (c) model level 16 (about 2455 m ASL), and (d) model level 23 (about 5565 m ASL, $\delta^{18}O_r$ (‰) at (e) 542 m ASL and (f) 2455 m ASL, and $\delta^{18}O_s$ (‰) at 5565 m ASL at 20 UTC on 15 October 2012. Note that due to the terrain-following coordinates, the SWI values are partly depleted over the topography, e.g. in central Italy. The precipitating area is marked by the area enclosed by the dashed line.

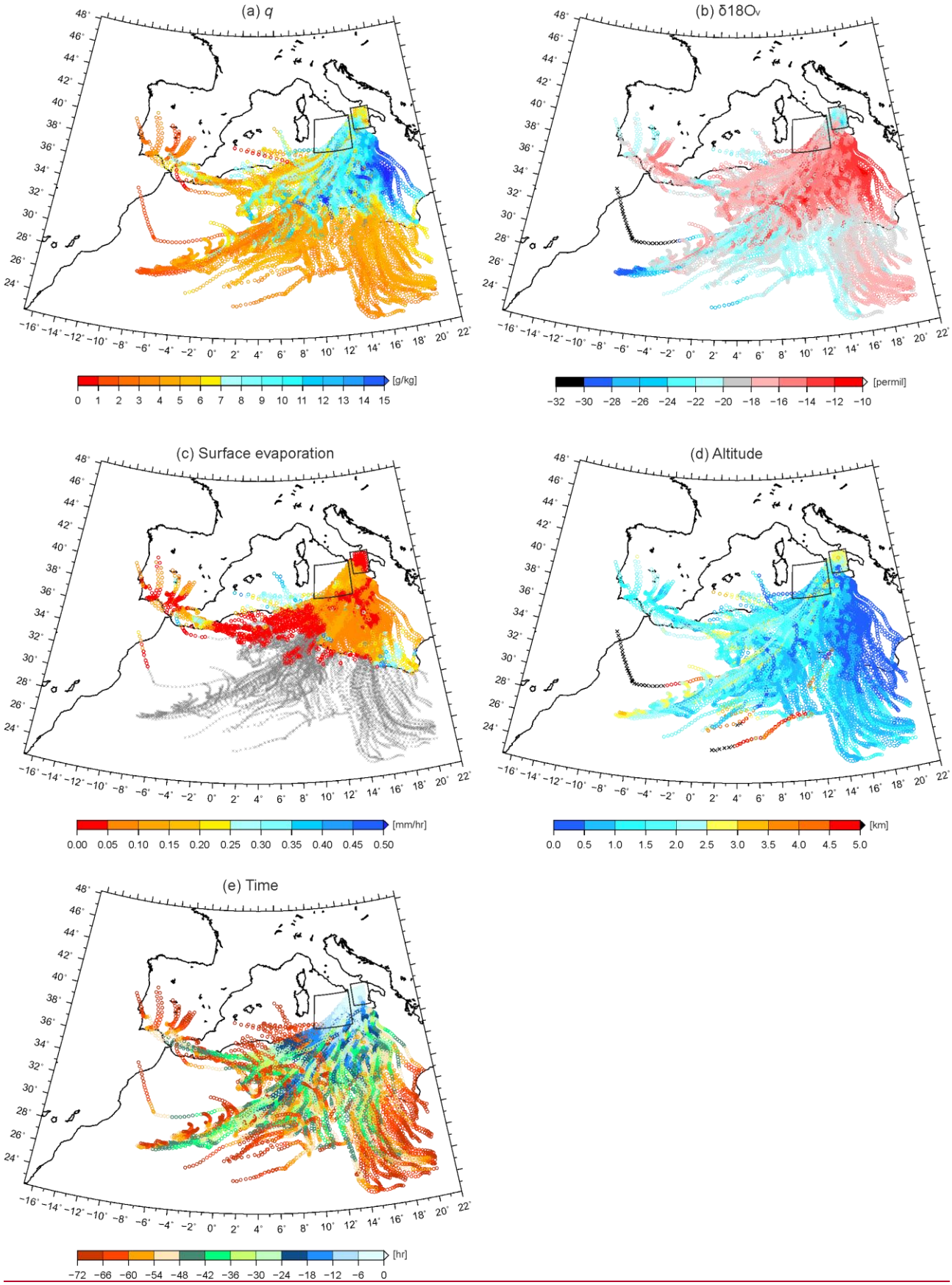

Figure 11. Same as Figure 7 but for the air parcel arriving at SI in layer of 800−700 hPa at 00 UTC on 16 October 2012.

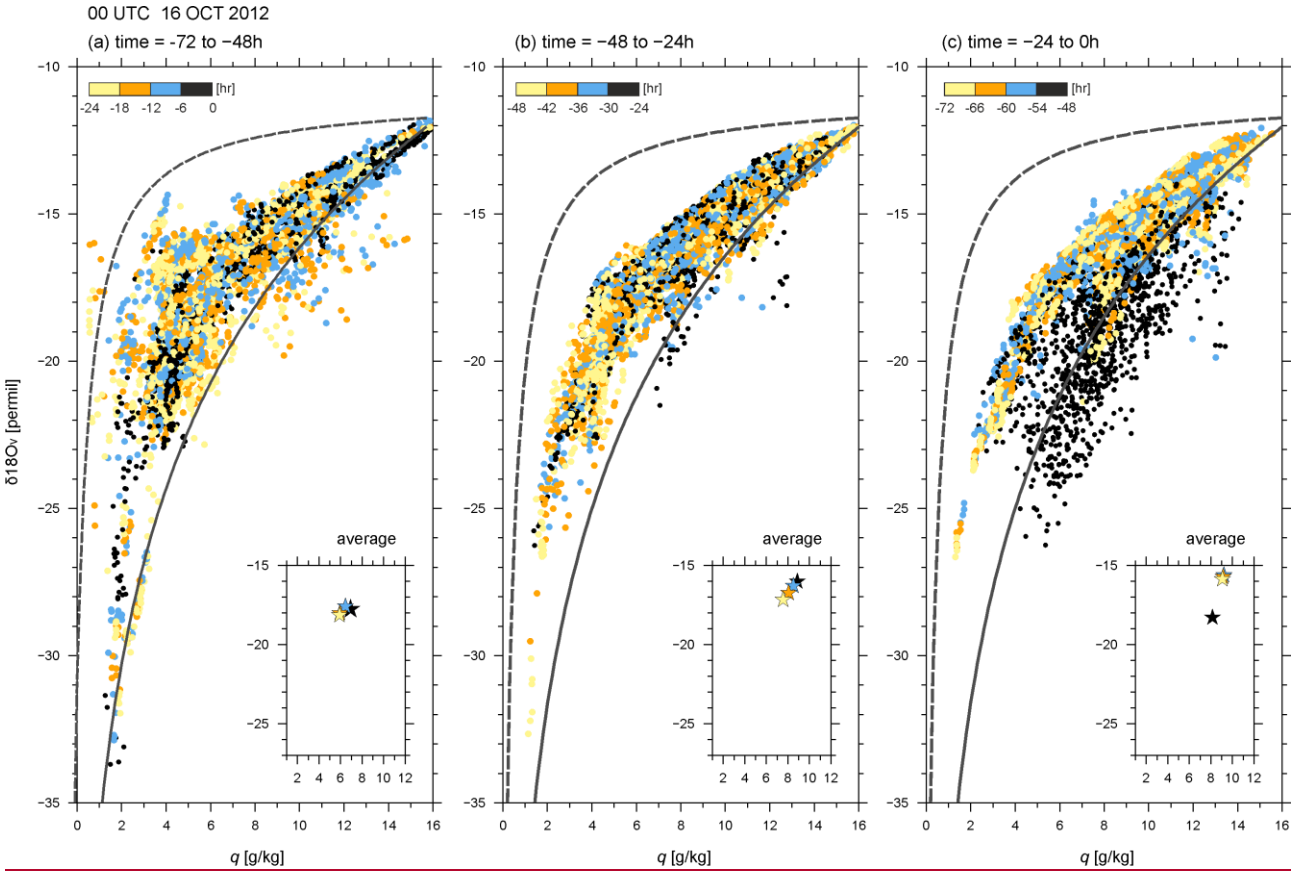

Figure 12. Scatter diagram of q and $\delta^{18}O_v$ along the backward trajectories of Figure 11 during (a) the times between −72 and −48 h~~r~~, (b) times between −48 h~~r~~ and −24 h~~r~~, and (c) times between −24 h~~r~~ and 0 h~~r~~ from 00 UTC on 16 October 2012 every 6 hours. The colour of dot changes every 6 h. The mixing and Rayleigh lines are indicated by ~~orange~~ dashed ~~line~~ and ~~blue~~ solid line, respectively. The averaged q and $\delta^{18}O_v$ every 6 hours is displayed in the bottom right corner of each panel.

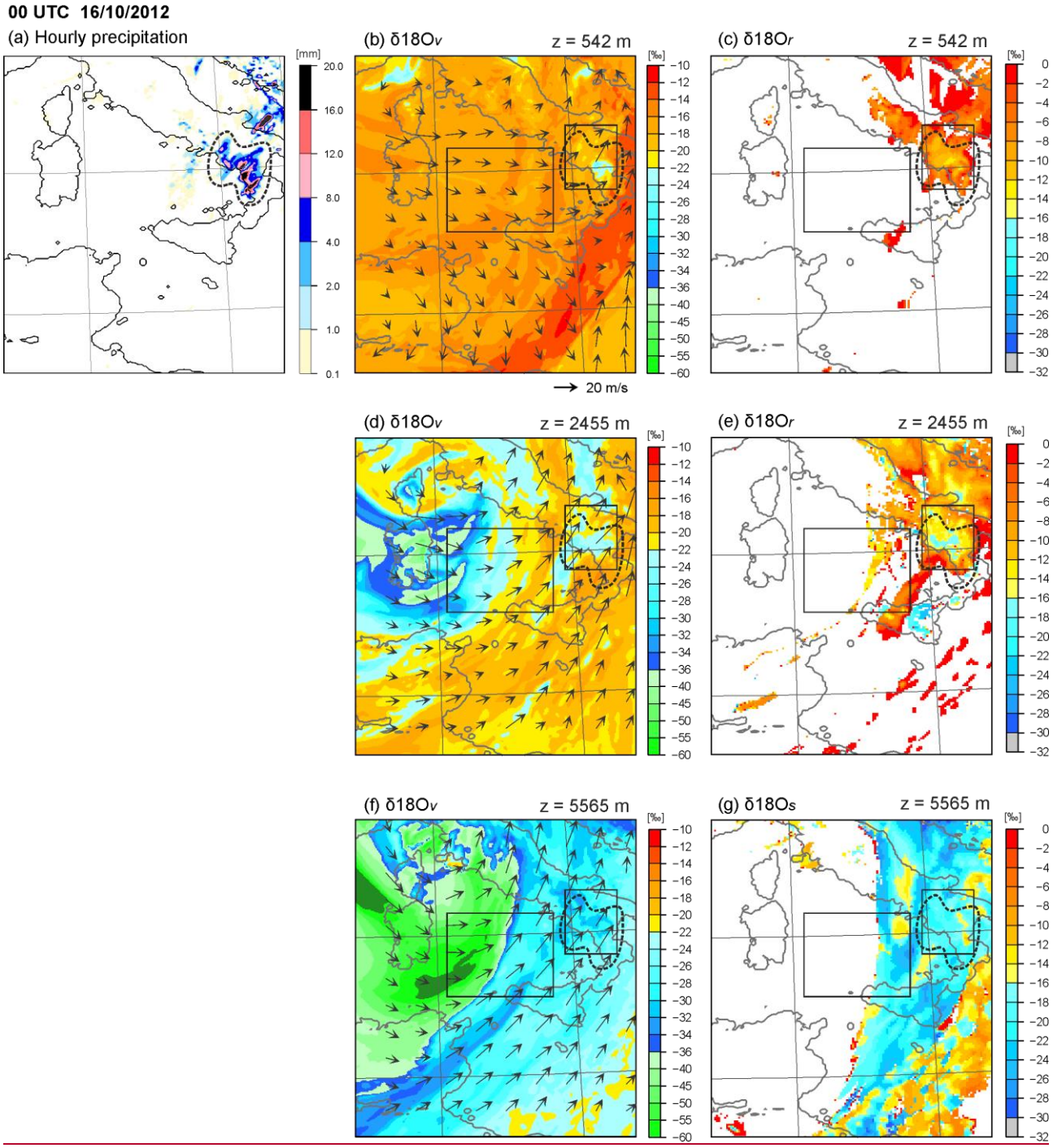

Figure 13. Same as Figure 10 but for 00 UTC on 16 October 2012.

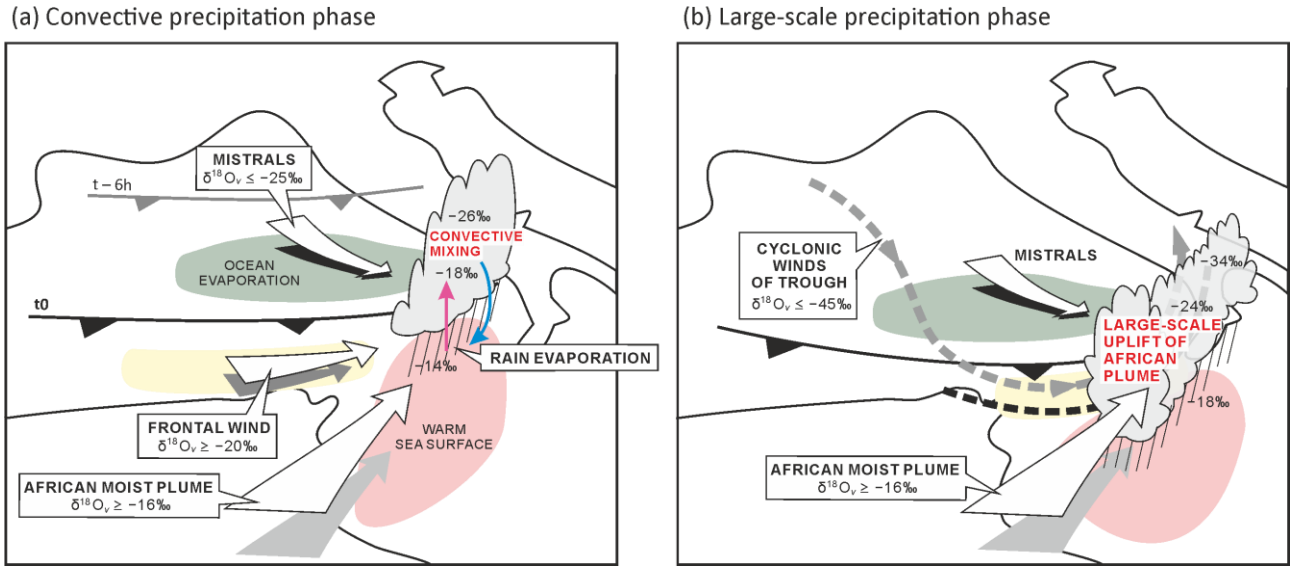

Figure 14. Schematics summarizing the main features of water vapour isotopologues and processes for deep convection upstream of SI and leading to the Phase 1 (a) and Phase 2 (b) of the HPE. In (a) and (b), white descending arrow indicate the mistral wind behind the edge of the cold front (thick black line). The white arrow in the yellow-shading encapsulated area illustrates the frontal wind at 850 hPa, and white arrow in the ~~blue~~red-shading encapsulated area (warm sea surface) indicates the elevated African moist plume. In (a), convective ascent and precipitating downdraft is depicted by red and blue arrows, respectively. In (b), the southern edge of upper trough is indicated by black dashed line and the cyclonic flow of the trough is indicated by grey dashed line.